Alma Mater Studiorum · Università di Bologna

Scuola di Scienze
Corso di Laurea Magistrale in Fisica

OPTICAL POWER STABILIZATION OF A LASER DIODE FOR QND MEASUREMENT

Relatore:
Prof. Elisa Ercolessi

Presentata da:
Michael Chong

Sessione II
Anno Accademico 2012/2013

"*If one tries to force the atoms or ions to behave as exact two-level objects one has to struggle hard with experimental difficulties which, in real life, conspire to blur these simple pictures*"

Haroche, S.

Raimond, J.M.

"Exploring the Quantum

Atoms, Cavities, and Photons"

"*It may sound crazy if you've learned too much quantum mechanics*"

Steinberg A.

Abstract

La realizzazione di stati non classici del campo elettromagnetico e in sistemi di spin è uno stimolo alla ricerca, teorica e sperimentale, da almeno trent'anni. Lo studio di atomi freddi in trappole di dipolo permette di avvicinare questo obbiettivo oltre a offrire la possibilità di effettuare esperimenti su condesati di Bose Einstein di interesse nel campo dell'interferometria atomica. La protezione della coerenza di un sistema macroscopico di spin tramite sistemi di feedback è a sua volta un obbiettivo che potrebbe portare a grandi sviluppi nel campo della metrologia e dell'informazione quantistica.

Viene fornita un'introduzione a due tipologie di misura non considerate nei programmi standard di livello universitario: la misura non distruttiva (*Quantum Non Demolition-QND*) e la misura debole. Entrambe sono sfruttate nell'ambito dell'interazione radiazione materia a pochi fotoni o a pochi atomi (*cavity QED* e *Atom boxes*). Una trattazione delle trappole di dipolo per atomi neutri e ai comuni metodi di raffreddamento è necessaria all'introduzione all'esperimento BIARO (acronimo francese Bose Einstein condensate for Atomic Interferometry in a high finesse Optical Resonator), che si occupa di metrologia tramite l'utilizzo di condensati di Bose Einstein e di sistemi di feedback. Viene descritta la progettazione, realizzazione e caratterizzazione di un *servo controller* per la stabilizzazione della potenza ottica di un laser. Il dispositivo è necessario per la compensazione del *ligh shift* differenziale indotto da un fascio laser a 1550*nm* utilizzato per creare una trappola di dipolo su atomi di rubidio. La compensazione gioca un ruolo essenziale nel miglioramento di misure QND necessarie, in uno schema di feedback, per mantenere la coerenza in sistemi collettivi di spin, recentemente realizzato.

Contents

Introduction

Since the early days of quantum physics the wave-particle duality that characterizes the quantum world has inspired the formulation of thought experiments involving single particles and single photons to explore and exploit their quantum nature. Perhaps the most famous of these experiments, the *photon box*, animated the debate between Einstein and Bohr at the VI Congress of Solvay in 1930. Famous paradoxes have arisen from the quantum world, including the renowned Schrödinger's cat. This example brings to our eyes the astounding consequences of the superposition principle applied to macroscopic systems and has inspired a theory of the decoherence phenomena. The Einstein Podolsky Rosen paradox, proposed in 1935, has lead to the formulation of hidden variables theories and to Bell inequalities, and opened a debate about the principle of locality in quantum theory.

From the 1980s, scientific and technological improvement gave physicists the chance to implement real experimental setups to perform those thought experiments and to test many crucial points of quantum theory. In the field of atomic physics such improvements include *ion traps*, *dipole traps* and *laser cooling*.
The 2012 Nobel Prize in physics to D.J. Wineland and S. Haroche "for groundbreaking experimental methods that enable measuring and manipulation of individual quantum systems"[1] is the latest of a list of prizes for works in this field of physics, that embraces the study of cold atoms, of interferometry, metrology and the fundamental properties of the quantum world such as the measurement

[1] "The Nobel Prize in Physics 2012". Nobelprize.org.

process.
Quantum nondemolition (QND) measurement, first proposed in the 1970's for the detection of gravitational waves [14], is a special type of measurement process in which the uncertainty of the measured observable does not increase from its measured value during the subsequent normal evolution of the system. QND measurements allow to attain the true nature of quantum measurements: after the measurement process the system is collapsed in an eigenstate of the measured observable and subsequent measurements will find the system in the same eigenstate.
Recently single photons stored in a cavity have been measured without being adsorbed by a detector using QND measurements [44]; Fock states have been generated in a controlled way in solid state systems [31]; non classical states of light have been prepared through feedback schemes that rely on QND measurements [51].

In the BIARO (French acronym for *Bose Einstein condensate for Atom Interferometry in a high finesse Optical Resonator*) experiment, Rubidium atoms are trapped and cooled in a high finesse cavity. Ensembles of atoms are treated as pseudo spin system and the coupling with laser radiation allows to reach all optical BEC and to perform QND measurement of the population of the outermost electronic levels. Recently it has been proposed a theoretical scheme for the realization of *spin squeezed states* and *Dicke states* [54] using QND measurements and a feedback scheme to preserve coherence of a collective spin state [55] has been realized.

In such a dynamic context, the evolution of electronics, of microcontrollers and of fast responding and low noise systems, is of central importance and has been fundamental for the realization of many experiments that were unimaginable only fourty years ago.
Such a rapid development opens now the door to new discoveries and to the evolution of promising technology such as *quantum computer*. Furthermore *weak measurements* may allow the complete measurement of the wavefunction. The *engineering* of *non classical states* of matter and of light that may be used to

improve the quality of interferometers and of atomic clocks.

Outline of the thesis

This Master thesis work has been done at the *Institut d'Optique* in the *Atom Optique* group on the BIARO experiment.
The experiment focuses on quantum metrology and investigates several technologies like: optical trapping of cold atoms, Bose Einstein condensates of Rubidium 87, weak measurement and feedback to protect an ensemble from the naturally occurring decoherence.

The first chapter is an introduction to measurements in quantum mechanics, starting from the *postulates* that define the measurement, following with the definition of QND measurements and eventually treating the weak measurement.

The second chapter introduces to the *dipole force*, that may be used to trap atoms with lasers: starting from the atom-field interaction the *dressed states* approach gives a great way to visualize what happens when single photons interact with single atoms treated first as two-level systems.

The third chapter is a review of theoretical aspects of *optical dipole traps*, common methods used to trap and techniques to cool neutral atoms. In particular *red-detuned* dipole traps for neutral atoms are treated.

The first three chapters serve as introduction for the in depth description of the BIARO experiment that is given in the fourth chapter. The experimental apparatus, the results concerning the realization of all optical Bose Einstein condensates and the engeneering of collective spin states through QND measurement are given, as well as the description of a feedback scheme recently developed.

My thesis work concerned the realization of a *servo controller* for the power of a fiber laser. The work has been driven by the necessity of a tuneable and stable optical power of a laser source aimed to improve QND measurements on trapped atoms. Chapter five is devoted to the conception and realization of such a device.

Chapter 1

MEASUREMENTS IN QUANTUM MECHANICS

We know from any quantum mechanics textbook that when we perform a measure on a system the wavefunction collapses on an eigenstate of the operator we are looking at. After collapsing the weavefunction evolves in time following the time tependent Schroedinger equation.
An example of measurement is the detection of a photon is using a photomultiplier: in the process the photon is adsorbed. This kind of measurement is called a *destructive* measurement because the system we were looking at is not just projected in the detected eigenstate of the operator, but essentially it is destroyed.
In the extreme case where the light field may contain either one or no photons when we measure the presence of that photon we leave the field *empty* (see section 1.2). The measurement makes the system collapse in a state which is different from the one we measured.

In this chapter we will focus on the notion of measurement in quantum mechanics starting from the postulates of quantum measurement in section 1.1. In the section 1.4 we define and discuss the weak measurement as defined by Aharonov [2] and as used later.
Finally in the last section we present and discuss the model of Quantum Non

Destructive[1] measurement and how can we use it to obtain information from a quantum system without destroing it.

This chapter is meant to be a brief introduction at the theoretical aspects that lie behind the work of the BIARO experiment.

1.1 Postulates of measurement

We start by the postulates of measurement as given in the book from Cohen-Tannoudji and Laloe [20]. There it is possible to find a comprehensive discussion of the postulates, their *physical interpretation* and a detailed mathematical discussion[2].

First postulate: at a fixed time t_0 the state of a physical system is defined by specifing a *ket* $|\psi(t_0)\rangle$ belonging to the state space Σ.

Second postulate: every measurable physical quantity $\mathscr{A}$ is described by an operator A acting in Σ; this operator is an *observable*.

Third postulate: the only possible result of a measurement of a physical quantity $\mathscr{A}$ is an eigenvalue of the corrisponding observable A.

Fouth postulate (discrete spectrum): when the physical quantity $\mathscr{A}$ is measured on a system in the *normalized* state $|\psi\rangle$, the probability $\mathscr{P}(a_n)$ of obtaining the eigenvalue a_n of the corresponding observable A is

$$\mathscr{P}(a_n) = \sum_{i=1}^{g_n} |\langle u_n^i | \psi \rangle|^2$$

where g_n is the degeneracy and the $|u_n^i\rangle$ form a set of orthonormal vectors which form a basis in the eigensubspace Σ_n associated with the eigenvalue a_n.

[1] Often reported as quantum non demolition or QND.

[2] Our discussion of the postulates is deliberately non-technical from the mathematical point of view.

Fifth postulate: if the measurement gives the result a_n the state of the system *immediately* after the measurement is the normalized projection onto the eigensubspace associated with a_n: $\frac{P_n|\psi\rangle}{\sqrt{\langle\psi|P_n|\psi\rangle}}$.

Sixth postulate: the time evolution of the state vector $|\psi(t)\rangle$ is governed by the Schroedinger equation:

$$i\hbar\frac{\mathrm{d}}{\mathrm{d}t}|\psi(t)\rangle = H(t)|\psi(t)\rangle$$

.

It is the fifth postulate, otherwise described as the reduction of the wave packet, that stresses out the concept that goes under the name of *projective* measurement. The meaning is simple and at the same time extremely important: before performing a measurement we should think in terms of probability to find a given result; this is due to the intrinsic nature of quantum mechanics and it is a consequence of the superposition principle[3]. But *right after* performing a measurement we do know in which particular state the system is: this is exactly the information we aquire through the measurement. If we could repeat it quickly enough we will get the *same* result. The time scale is fixed by the sixth postulate, the Schroedinger equation that tells us how the system will evolve with time.

1.2 Photodetection

Let's describe what happens when we measure how many photons are there in a certain field. The standard way of doing this kind of measurement is in striking contrast with the projection postulate.

When we perform a photo-detection process applied to a field mode, the measured quantity is the photon number operator $\hat{N} = \hat{a}^\dagger\hat{a}$. The eigenvalues of this operator are the the natural numbers and the eigenstates associated are the well

[3]Which is implicit in the first postulate, given that we provide a correct mathematical definition of the state space.

known Fock states with a definite number of photons. The counting of the photons, however, relies on the conversion of the photons into electric charges through the photo-electric effect. Therefore the measured photons are destoyed in this process. The effect of the measurement is to project the state into the vacuum instead of projecting it into a random photon number state as required by the projection postulate. This kind of measurement does not "project" the state: it "demolishes" it. This kind of measurement takes therefore the name of demolition measurement.

The destruction of the state is not required by the measurement postulates; it is then natural to ask ourself if is it possible to perform measurements which do not demolish the state. A measurement that has the effects we expect from the postulates.

In the limiting case of a field that may contain either one or no photons we should ask ourself if is it possible to *see* the same photon more than once. This question leads us into the domain of quantum non-demolition measurement that we are going to treat in section 1.3.

1.3 Quantum Non Demolition measurements

A comprehensive introduction to QND may be found in [13]; from the historical point of view it may be interesting to note that the first proposal of this kind of measurement were made in the context of gravitational wave detection in the 1970's by Braginsky and Vorontosov.

Following the textbook approach of Haroche and Raimond [29] we start by stating the properties of a QND measurement: it is a detection process wich *projects* the state of the system into the eigenstate corresponding to the result of the measurement instead of erasing entirely the information of the state it has detected. The second essential feature in the definition of a QND process is the *repeatability*: two successive measurement should yeld the same result[4].

[4]Given that the system has not evolved in the meantime due to some kind of perturbation or a 'long' time evolution

Let's point out that this kind of measurement are the only measurement that follow strictly the postulates of measurement: this are the only *true* quantum measurements.

1.3.1 Conditions for QND

Here we state the conditions for a measurement to be QND.
Suppose we have a system S and that we want to measure an observable O_S of this system. The mechanism relies on the coupling of the system with a meter M that evolves among an ensemble of *pointer* states each *"pointing towards"* an eigenvalue of O_S. The ensemble of this pointing states should form an eigenbasis of an observable of the meter O_M. The full Hamiltonian takes the form:

$$H = H_S + H_M + H_{SM}, \tag{1.1}$$

where the third term is the coupling between the system and the meter. The conditions for QND are that:

1. there must be some information about O_S encoded in the pointer states *after* the interaction: the system-meter interaction Hamiltonian must not commute with the meter observable.

   $$[H_{SM}, O_M] \neq 0.$$

   This is a *necessary* condition that ensures that the interaction has some effect on the evolution of the meter.

2. The measurement should not affect the eigenstates of O_S. Often it is easier to express this condition in a *sufficient* form[5]:

   $$[H_{SM}, O_S] = 0.$$

[5]For a detailed discussion of this point, including the necessary form of this condition, refer to [13].

3. The measurement must be repeatable; excluding extremely fast processes we can require that the observable of the system should be an integral of motion for the free system Hamiltonian:

$$[H_S, O_S] = 0.$$

The latter condition tells us that some quantities may never be measured in a QND way; the simplest exemple is the coordinate X of a free particle in a one dimensional motion: here the free Hamiltonian is proportional to P^2 and therefore does not commute with $O_S = X$. In this situation we have a huge 'back-action' of the measurement on the system that makes it impossible to repeat the measurement and get the same result: if with the first detection we project the system into a position eigenstate, according to Heisenberg uncertainity relation, the state has infinite momentum dispersion. Therefore during the time between two subsequent measurement we have an evolution of the system that have the effect of a complete dispersion of the results obtained for X.

1.3.2 Single-photon measurement

It may be useful to follow how a QND measurement is done in a specific situation. In [29] there are several ones discussed both theoretically and from an experimental point of view. Here we report part of the discussion about the detection of the presence of a single photon in a cavity using a Rydberg circular atom[6] with a standard cavity QED setup using a Ramsey interferometer as in picture 1.1a.

The QND meter is a single Rydberg atom; three states with different principal quantum number $|e\rangle$, $|g\rangle$ and $|i\rangle$ are involved. The coupling is provided by the resonant vacuum Rabi oscillation[7] on the $|e\rangle \rightarrow |g\rangle$ transition. The atom-cavity interaction time t is set for a 2π Rabi pulse on this transition.

[6] Rydberg atoms have high principal quantum number and in their circular configuration the atomic angular momentum may reach macroscopic values.

[7] For a discussion about the Rabi problem see section 2.1.

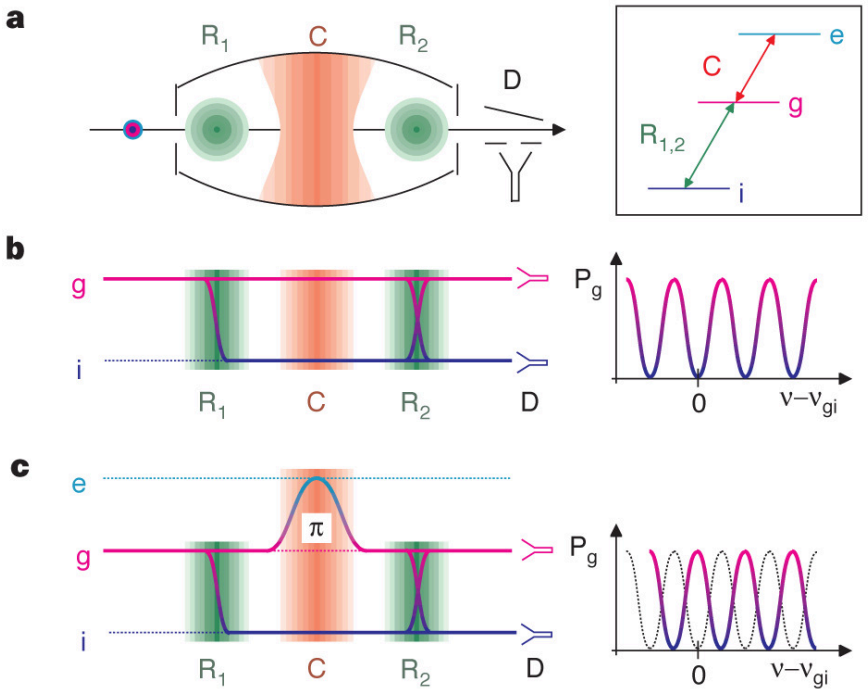

Figure 1.1: a) Atoms cross the cavity C one at a time; the cavity mode (shown in red) stores the field to be measured. The e, g and i atomic levels are shown in the inset. The cavity mode is resonant with the $e \rightarrow g$ transition. Atoms are subjected in zones R_1 and R_2 (in green) to auxiliary pulses (frequency ν), quasi-resonant with the $g \rightarrow i$ transition (frequency ν_{gi}). Detector D, downstream, measures the states of the atoms. b) Diagram depicting the interfering paths followed by an atom initially in g when there is no photon in the cavity mode. The atom travels between R1 and R2 either in g (violet line) or in i (blue line). The probability amplitudes associated with these two paths interfere, leading to fringes in the probability P_g of detecting the atom in g when ν is scanned (shown at right). c) As b but when the cavity mode stores one photon. The atom, if in level g, undergoes a full reversible cycle of photon absorption and emission, finally leaving the photon in C. In the process, the corresponding amplitude has undergone a π phase shift and the fringes are reversed (as shown at right). Image and caption taken from [44].

If the atom is initially in $|g\rangle$ and there is one photon the atom-field system undergoes a complete oscillation passing through $|e\rangle$ and comes back, up to a phase shift, to the initial state when the atom leaves the cavity. The state, depending on the presence of the photon, may undergo one of the following transformations:

$$|g,1\rangle \to -|g,1\rangle;\ |g,0\rangle \to |g,0\rangle,$$

where $|n=1\rangle$ ($|n=0\rangle$) represent the presence (absence) of a photon.
What is remarkable is that the presence of a photon produces a π-phase shift of the atomic state; the information is stored into the atom without destroying the photon making this a genuine QND process.

The atomic state $|i\rangle$ comes into play to detect this phase shift: the transitions from this level to the $|g\rangle$ level are far detuned from the cavity mode so that this state stays invariant passing through the cavity; it is therefore possible to use it as a phase reference.

The complete procedure to obtain the information about the cavity is the following: first, a $\pi/2$ microwave pulse is applied to the atom before it enters the cavity, so as to put it in a coherent superposition of the $|g\rangle$ and $|i\rangle$ states:

$$|g\rangle \to (|g\rangle + |i\rangle)/\sqrt{2}. \tag{1.2}$$

The atom then passes through the cavity and is later probed at the end exit of it using a second $\pi/2$ pulse that *completes* the Ramsey interferometer setup realizing the transformations:

$$|g\rangle \to \frac{(|g\rangle + e^{i\phi}|i\rangle)}{\sqrt{2}};\ |i\rangle \to \frac{(|i\rangle - e^{-i\phi}|g\rangle)}{\sqrt{2}}. \tag{1.3}$$

Adjusting the microwave pulse around the $|i\rangle \to |g\rangle$ transition it is possible to tune the relative phase ϕ; the probability $P_{g|n}$ of finding the atom in the state $|g\rangle$ depends on the presence of the photon in the cavity:

$$P_{g|0} = (1-\cos(\phi))/2; \tag{1.4a}$$

$$P_{g|1} = (1+\cos(\phi))/2, \tag{1.4b}$$

If we choose the relative phase to be 0 it is easy to see that the probability to find the atom in the ground state is 0 if there are no photons in the cavity and 1 if

there is one. Therefore we have a way to detect the presence of the photon in the cavity. Is the state of the system destroyed after the measurement? When there are initially no photons in the cavity nothing happens: the atom was in the $|g\rangle$ state before entering the cavity and remains in the same state. The cavity remains *empty*. What happens to the photon if the cavity is not empty in the beginning? The Rydberg atom enters the cavity, absorbs the radiation and goes transiently through $|e\rangle$ before finally returning to $|g\rangle$ and releasing the photon. Therefore in the cavity there was a photon in the beginning and there remains one when the atom leaves the cavity.
Single photon cavity QND has been realized and a complete discussion of the (many) experimental subtleties may be found in Nouges et al 1999 [44].
Let's stress out that this simple configuration is so effective only if the cavity is in the subspace spanned by $|0\rangle$ and $|1\rangle$: if the cavity is allowed to be in a Fock state with more than one photon the 2π Rabi rotation is not exact anymore and there is probability of absorbing one photon after the complete rotation. We restrict to this simple situation which presents all the elements of a QND and we will not discuss the methods to realize a QND measurement of this type for a broader Fock subspace.

1.3.3 Standard Quantum Limit

One of the feature of QND measurement is that it makes possible to overcome the standard quantum limit (SQL). We know from the Heisenberg uncertainity principle that we cannot measure at the same time a pair of conjugate variables A and B with arbitrary precision:

$$\Delta A \Delta B \geq \hbar.$$

Anyway nothing prevents us from detecting one of the variables with arbitrary precision at the price of losing information on the conjugate. The SQL has to do with the *continuous* observation of a variable and in this section we discuss a simple example to introduce what this limit is following [13].

Suppose that the coordinate $x(t)$ of the mass of an oscillator with eigenfrequency ω is *continuously* monitored. The value $x(t)$ may be expressed by two quadrature amplitudes X_1 and X_2 related to x by:

$$x(t) = X_1 \cos(\omega t) + X_2 \sin(\omega t). \tag{1.5}$$

The measurement errors satisfy the uncertainity relation:

$$\Delta X_1 \Delta X_2 \geq \frac{\hbar}{2m\omega}. \tag{1.6}$$

The continuous monitoring of the coordinate is equivalent to the simultaneous measurement of the quadrature amplitudes with symmetrical uncertainity $\Delta X_1 = \Delta X_2$. If we substitute the symmetrical uncertainity condition in equation 1.5 we obtain the standard quantum limit fo the coordinate of the oscillator:

$$\Delta_{SQL} = \sqrt{\frac{\hbar}{2m\omega}}. \tag{1.7}$$

Different physical systems and observables have different SQLs and some examples are given in [13] and in the references cited therein.

QND measurements allows us to extract information *only* on a single observable disturbing noncommuting ones precisely to the extent that provides satisfaction of the uncertainity principle. Using Braginsky's words:

> [...] the ideal QND measurement is an exact one: the meter does not add any perturbation, and possible variance is the consequence of the *a priori* uncertainity of the value to be measured.

1.4 Weak measurements

In this last section we introduce the concept of *weak measurement* first proposed by Aharonov et al. in 1988 in [2]. The idea of realizing this kind of measurement is becoming very common and there are several experiments nowadays that use this procedure to obtain information with a probe characterized by a reduced strenght. An interesting and non technical review of these experiments may be found in [16] while a detailed one is [12].

Weak measurement is a generalization of the projective measurement that relies on a weak coupling between the system and the meter to gather some information about the system almost without perturbing it. The meter is usually a quantum object and to obtain the *weak value of a quantum variable* of the system we have to perform a *strong* measurement on the meter.

The standard measurement procedure has an Hamiltonian of the type [56]:

$$H = -g(t)Q_M A_S, \tag{1.8}$$

where $g(t)$ is a normalized function with a compact support near the time of measurement t; Q_M is a canonical variable of the meter with conjugate variable P_M[8] and A_S is the observable we want to measure.

In an ideal situation the initial state of the meter has a well defined P_M value p. The value of A_S after the interaction described by H is related to the final value of P_M.

In real situations we may assume the initial state of the meter to be a Gaussian in the Q_M and P_M representations. Therefore, if the initial state of the system is $\sum_i a_i|A_S = a_i\rangle$, the Hamiltonian (1.8) evolves the system to:

$$e^{-i\int H\mathrm{d}t} e^{-p^2/4(\Delta p)^2} \sum_i a_i|A_S = a_i\rangle = \sum_i a_i e^{-(p-a_i)^2/4(\Delta p)^2}|A_S = a_i\rangle. \tag{1.9}$$

If Δp is much smaller than the spacing between the eigenvalues a_i then after the measurement we shall be left with the mixture of Gaussians located around a_i correlated with different eigenstates of A_S. A measurement of P_M will then indicate the value of A_S.

What if the Δp is much bigger than all a_i? The final probability distribution will still be a Gaussian but now we have a huge spread. The center of the Gaussian will be at the mean value of A_S: $\langle A_S\rangle = \sum_i |a_i|^2 a_i$. A single measurement like this will give us almost no information because the spread of the Gaussian is much higher than the $\langle A_S\rangle$.

If we want to measure the value of A_S of a particle in an ensemble of N particles prepared in the *same* state we can reduce the relevant uncertainity by the

[8] They satisfy $[Q_M, P_M] = i\hbar$.

factor $1/\sqrt{N}$ leaving unchanged the mean value of the average $\langle A_S \rangle$. Enlarging the number N we can obtain a measurement with the desired precision.

1.4.1 Postselection

For a sufficiently large ensemble, as said in the previous section, we are able to obtain the value $\langle A_S \rangle$ by taking the average of the outcome of the strong measurement of P_M.
We may now change the outcome of $\langle A_S \rangle$ by averaging on a particular subensemble and taking account only of the values of P_M of this part of the original ensemble *after* the measurement has been done. We call the operation of chosing the subensemble a *postselection*. Surprisingly enough some postselections about the particles may yield values of $\langle A_S \rangle$ outside the expected range $[min(a_i), max(a_i)]$.
The procedure of the measurement starts with a large ensemble of particles prepared in the same initial state. Every particle should interact with a *separate* measuring device. Then we perform the measurement wich selects the final state. In the end we take into account only the values of P_M corresponding to the postselected particles.

Consider an ensemble of particles with initial state $|\psi_i\rangle$ and a final state $|\psi_f\rangle$. In between we switch on the interaction described in eq.1.8 with an initial state of the meter proportional to $e^{-q^2/4\Delta^2}$. After the postselection the state of the meter (up to a normalization factor) is

$$\langle \psi_f | e^{-i\int H \mathrm{d}t} | \psi_i \rangle e^{-q^2/4\Delta^2} \cong \langle \psi_f | \psi_i \rangle e^{iq\frac{\langle \psi_f | A_S | \psi_i \rangle}{\langle \psi_f | \psi_i \rangle}} e^{-q^2/4\Delta^2}. \tag{1.10}$$

The congruence holds if the spread Δ is sufficiently small:

$$\Delta \ll max_n \frac{|\langle \psi_f | \psi_i \rangle|}{|\langle \psi_f | A_S^n | \psi_i \rangle|^{1/n}}. \tag{1.11}$$

In the p representation the state of the meter after the postselection is approximately

$$exp[-\Delta^2 (p - \frac{\langle \psi_f | A | \psi_i \rangle}{\langle \psi_f | \psi_i \rangle})^2];$$

this state gives us the *weak value* for A_S:

$$A_{S_W} \equiv \langle \psi_f | A | \psi_i \rangle / \langle \psi_f | \psi_i \rangle. \tag{1.12}$$

It is important to stress out that the uncertainty of p for each of the meters is much bigger than the measured value: $\Delta p = \frac{1}{2}\Delta \gg A_{S_W}$ therefore a single measurement does not provide a precise information about the observable A_S. But the average on N system+meter devices allows us to come to the situation where $\Delta p/\sqrt{N} \ll A_{S_W}$ and is therefore possible to ascertain the value of A_{S_W} with arbitrary precision.
A discussion of the mathematics beheind the weak value may be found in the original paper by Aharonov [2] and in [3]. Weak measurement has opened the doors for a deeper understanding of the quantum world but has also introduced some strangeness that we won't discuss here. For the interested reader there are recent experimental works (and open problems) about the possibility to measure the trajectories of particles passing through an interferometer [35] and about the complete measurement of a wavefunction [40]. In 1992 Lucien Hardy suggested a paradoxical thought experiment that uses weak measurements [28] and the first experimental realizations are now being published [58].

Chapter 2

DIPOLE FORCE

In this chapter we introduce the concept of dipole force raising from what is called the lighshift of the levels of an atom due to strong coupling with a light field. The basic idea is that an electromagnetic field can be used to shift the energy levels of an atom; the energy shift is dependent on the intensity of the beam (and therefore, in a real situation, on the shape of the beam and the position of the atom inside it). Due to this dependance of the energy shift on the position the atoms in a laser beam experience a force dependent on their position and the detuning of the laser with respect to the atomic frequency.
In section 2.1 we introduce the results of the Rabi two-level problem as a starting point for the following sections. We then expose in section 2.2 the main results of the *dressed states picture* that are very useful to visualize radiation pressure and dipole force acting on atoms in a laser field.

2.1 Atom-Field interaction

Consider an atom in a radiation field: the time evolution of the system is given by the time dependent Schroedinger equation:

$$\hat{H}\psi(\overrightarrow{r},t) = i\hbar\frac{\partial\psi(\overrightarrow{r},t)}{\partial t}, \tag{2.1}$$

where $\hat{H}$ is the *total* Hamiltonian for the atom in the field which is given by a field free, time indipendent, atomic part $\hat{H}_0$ and the interacting part $\hat{H}_i(t)$. The field free part have eigenvalues $E_n = \hbar\omega_n$ and eigenfunctions $\phi_n(\overrightarrow{r})$ which form a complete set that can be used to expand the solution of 2.1:

$$\psi(\overrightarrow{r},t) = \sum_k c_k(t)\phi_k(\overrightarrow{r})e^{-i\omega_k t}. \tag{2.2}$$

If we substitute the expansion in 2.1, after a simple manipulation[1] we get to the following system of equations that are *equivalent* to the starting equation:

$$i\hbar\frac{\mathrm{d}c_j(t)}{\mathrm{d}t} = \sum_k c_k(t)H'_{jk}(t)e^{-i\omega_{jk}t}, \tag{2.3}$$

where $H'_{jk}(t) = \langle\phi_j|\hat{H}'(t)|\phi_k\rangle$ and $\omega_{jk} = (\omega_j - \omega_k)$.

2.1.1 The Rabi two-level problem

To evaluate the solution of such a system in the case of our interest we can make the following approximations:

1. consider an atom with the inner shells filled, so that only two atomic levels are available in first approximation; this means that in 2.3 we can truncate the sum just to two levels, ground (k=1) and excited (k=2). This gives the Rabi two-level problem first studied in [47].

2. If we use a narrow band laser (with angular frequency ω_l) as a radiating field it is useful to make the *rotating wave approximation* (RWA) that consists in neglecting terms of the order $1/\omega_l$ compared to terms of the order $1/\delta$ where $\delta = \omega_l - \omega_a$ is the *detuning* of the laser compared to the atomic resonance frequency.

3. We may consider the the electric field $\mathscr{E}(\overrightarrow{r},t)$ to be constant in space in the region of interest: the wavelenght is typically of the order of 10^2nm compared to the dimension of the $\phi_k(t)$ that usually are contained in a radius $\leq$ 1nm. This results in the *electric dipole approximation*.

[1] For details in the derivation see, for instance, [43] and references cited therein.

As a result of the approximation we can obtain the *uncoupled* differential equations for the $c_g(t)$ and the $c_e(t)$:

$$\frac{\mathrm{d}^2 c_g(t)}{\mathrm{d}t^2} - i\delta\frac{\mathrm{d}c_g(t)}{\mathrm{d}t} + \frac{\Omega^2}{4}c_g(t) = 0, \tag{2.4}$$

$$\frac{\mathrm{d}^2 c_e(t)}{\mathrm{d}t^2} + i\delta\frac{\mathrm{d}c_e(t)}{\mathrm{d}t} + \frac{\Omega^2}{4}c_e(t) = 0; \tag{2.5}$$

here we introduced the *Rabi* frequency[2] Ω defined as

$$\Omega = \frac{-eE_0}{\hbar}\langle e|\hat{r}|g\rangle,$$

where E_0 is the amplitude of a light field in the form of a plane wave propagating in the z direction. To get an idea of what these equations imply let's look at the solution for the simple initial conditions $c_g(0) = 1$, $c_e(0) = 0$:

$$c_g(t) = \left(\cos\frac{\Omega' t}{2} - i\frac{\delta}{\Omega'}\sin\frac{\Omega' t}{2}\right)e^{+i\delta t/2}, \tag{2.6}$$

$$c_e(t) = -i\frac{\Omega}{\Omega'}\sin\frac{\Omega' t}{2}e^{-i\delta t/2}. \tag{2.7}$$

The generalised Rabi frequency Ω' is defined as:

$$\Omega' = \sqrt{\Omega^2 + \delta^2}.$$

The solutions clearly suggest that the electron is oscillating between the two levels with frequqncy Ω' that increases with the detuning δ. The probability to find the electron in the exicted state is proportional to $\frac{\Omega^2}{\Omega'^2}$ that is the amplitude decreases as we increase the detuning.

2.1.2 Introducing the Light Shifts

The effect of the field on the atom can be more subtle than what we considered until now. The energies E_n, eigenvalues of E_0 are no longer eigenvalues of the full Hamiltonian due to off-diagonal terms in H'.

[2]This definition of the Rabi frequency is made to be the real oscillation frequency of $|c_k(t)|^2$ in the case of exactly resonating field (i.e. $\delta = 0$).

If we evaluate the equations 2.3 using a time-*indipendent* perturbation H'_{ge} and absorb the time dependence $e^{-i\omega_k t}$ into each coefficient $c_k(t)$ we would get the following set of equations[3]:

$$i\hbar\frac{\mathrm{d}c'_g(t)}{\mathrm{d}t} = c'_e(t)\frac{\hbar\Omega}{2}, \tag{2.8}$$

$$i\hbar\frac{\mathrm{d}c'_e(t)}{\mathrm{d}t} = c'_g(t)\frac{\hbar\Omega}{2} - c'_e(t)\hbar\delta, \tag{2.9}$$

where the primed coefficients are related to the non primed ones by:

$$c'_g(t) = c_g(t),$$

$$c'_e(t) = c_e(t)e^{-i\delta t}.$$

The energies of the ground and excited states, shifted by the field, are therefore found diagonalizing the matrix of the system to obtain:

$$\Delta E_{e,g} = \hbar/2(-\delta \mp \Omega'). \tag{2.10}$$

2.2 Dressed states picture

The eigenstates corresponding to the $\Delta E_{g,e}$ are the so called *dressed states* discussed in [20]; as in the whole chapter we will briefly report the results of our intrest: for an insightful discussion refer to [23].

We start by writing the Hamiltonian for the atom-laser coupled system

$$\hat{H} = \hat{H}_A + \hat{H}_R + \hat{V} \tag{2.11}$$

with the three terms in their second quantized version:

$$\hat{H}_A = \frac{P^2}{2m} + \hbar\omega_a b^\dagger b; \tag{2.12}$$

here $b = |g\rangle\langle e|$ and $b^\dagger = |e\rangle\langle g|$ are the lowering and raising operators.

$$\hat{H}_R = \sum_\lambda \hbar\omega_\lambda a^\dagger_\lambda a_\lambda, \tag{2.13}$$

[3]There are different ways to get this result, including the *rotating frame transformation*; discussion of the different methods can be found in [43], in [8] or in the many references cited therein.

where $a_\lambda^\dagger$ and a_λ are the creation and destruction operators of a photon in the mode λ amongst which there is $\lambda = l$, the one corresponding to the laser field[4]. The interaction term is expressed (in the dipole approxmation and RWA) using the positive and negative frequency components of the electric field taken for the atomic average position $r = \langle \hat{r} \rangle$[5]:

$$E^+(r) = \sum_\lambda \mathscr{E}_\lambda(r) a_\lambda;$$

$$E^-(r) = \sum_\lambda \mathscr{E}_\lambda^\star(r) a_\lambda^\dagger.$$

The expression for the interaction is then just:

$$\hat{V} = -\overrightarrow{d}\,[b^\dagger E^+(r) + bE^-(r)]. \tag{2.14}$$

In the following we neglect the kinetic term in the atomic Hamiltonian[6]. When the atom laser mode coupling is not taken into account (i.e. $\overrightarrow{d} = 0$) we get a picture which is easy to visualize:
"the eigenstates of the dressed Hamiltonian are bunched in manifolds $\mathscr{E}_n$, n integer, separated by the energy $\hbar\omega_l$, each manifold consisting of two states $|g, n+1\rangle$ and $|e,n\rangle$"[23] separated by the energy $\hbar(\omega_a - \omega_l) = \hbar\delta$ as in figure 2.1a.

Introducing the atom-laser coupling further splits the energy of states belonging to the same manifold. It is possible to re-define the (real) Rabi frequency $\Omega(r)$ and to introduce a phase $\phi(r)$ related by[7] [8]:

$$\frac{2}{\hbar}\langle e,n|V|g,n+1\rangle = \Omega(r)e^{i\phi(r)}. \tag{2.15}$$

[4]The electromagnetic field is quantized on a complete set of orthonormal field distributions $\mathscr{E}_\lambda(r)$.

[5]A more complete treatment would use the position operator instead: the use of this semiclassical approssimation is valid as the extension Δr of the atomic wave packet is small compared with the laser wavelength λ.

[6]This is equivalent to solve the equations at a given point $\overrightarrow{r}$.

[7]The Rabi frequency defined in this way depends on the number of photons in the field. In a coherent laser field with Poissonian distribution and sufficiently large mean number of photons we can neglect the dependance and thus recover the previous definition.

[8]The definition given in section 2.1.1 for the generalized Rabi frequqncy holds.

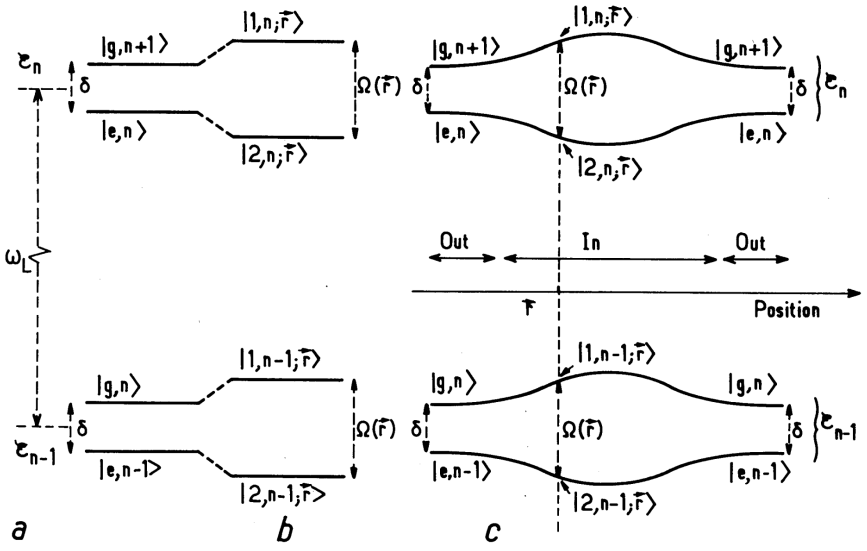

Figure 2.1: Dressed states energy leveles. a) Shows the energy levels for two different manifolds when the atom-laser mode is not taken into account. b) Effect of the laser-atom couplig on the energy levels. c) Position dependent energy levels in a gaussian laser beam: outside the beam we recover the situation of uncoupled states.. Image taken from [23].

The energies for the full dressed Hamiltonian are still folded in manifolds $\mathscr{E}_n$ (see fig.2.1b) but the coupled levels are now shifted by the amount found in the previuos section in eq. 2.10. It is now useful to sighty change the notation to better appreciate the dressed states formalism:

$$E_{1,2;n}(\overrightarrow{r}) = (n+1)\hbar\omega_L - \frac{\hbar}{2}\left(\delta \pm \Omega'(\overrightarrow{r})\right) \tag{2.16}$$

corresponding to the eigenstates:

$$|1,n;\overrightarrow{r}\rangle = +e^{i\phi(\overrightarrow{r})/2}\cos(\theta)|e,n\rangle + e^{-i\phi(\overrightarrow{r})/2}\sin(\theta)|g,n+1\rangle; \tag{2.17a}$$

$$|2,n;\overrightarrow{r}\rangle = -e^{i\phi(\overrightarrow{r})/2}\sin(\theta)|e,n\rangle + e^{-i\phi(\overrightarrow{r})/2}\cos(\theta)|g,n+1\rangle. \tag{2.17b}$$

Here the angle θ is position dependent and defined as:

$$\cos(2\theta(\overrightarrow{r})) = -\frac{\delta}{\Omega'(\overrightarrow{r})},\ \sin(2\theta(\overrightarrow{r})) = \frac{\Omega(\overrightarrow{r})}{\Omega'(\overrightarrow{r})}.$$

The importance of this result is due to two different facts:

1. the dressed states are combination of the ground and excited states of the bare Hamiltonian;

2. in an inhomogeneus laser field both the energies and the states will depend on the position of the atom in the field (figure 2.1c depicts the situation for a gaussian beam).

2.2.1 Spontaneous emission

Spontaneus emission in the dressed picture allows to easily interpret the triplet structure of the spontaneus emission in terms of a princpial band (frequency ω_L) and two sidebands (frequency $\omega_L \pm \Omega'(\overrightarrow{r})$).
Since states $|1,n;\overrightarrow{r}\rangle$ and $|2,n;\overrightarrow{r}\rangle$ are superposition of the ground and excited states of the bare Hamiltonian we have four possible couplings when we consider the pair of manifolds $\mathscr{E}_n$ and $\mathscr{E}_{n-1}$ that correspond to the three different frequencies. The matrix elements between $|j,n;\overrightarrow{r}\rangle$ and $|i,n-1;\overrightarrow{r}\rangle$ are the $d_{ij} = \langle i,n-1;\overrightarrow{r}|d(\hat{b}+\hat{b}^\dagger)|j,n;\overrightarrow{r}\rangle$:

$$d_{11} = -d_{22} = \overrightarrow{d}\cos(\theta)\sin(\theta)e^{i\phi}; \tag{2.18a}$$

$$d_{12} = -\overrightarrow{d}\sin^2(\theta)e^{i\phi}; \tag{2.18b}$$

$$d_{12} = \overrightarrow{d}\cos^2(\theta)e^{i\phi}. \tag{2.18c}$$

Here the diagonal terms correspond to the principal band as it is easy to infer from figure 2.2.

2.2.2 Radiation pressure and dipole force

Now that the states are defined and the possible interaction delined it would be possible to study the evolution of the density operator ρ writing a master equation for the populations $\Pi_i(\overrightarrow{r})$ and coherences $\rho_{ij}(\overrightarrow{r})$ as function of the rates of transfer Γ_{ij} (that are proportional, as one would expect, to the square of dipole matrix elements d_{ij}). This goes over the purpose of this work and we suggest the

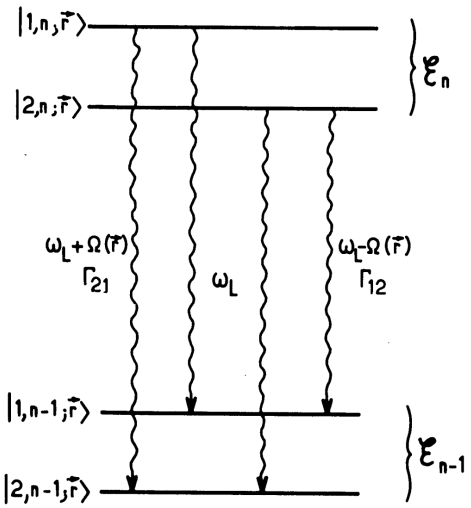

Figure 2.2: Spontaneus emission between dressed states and corresponding frequencies. Image taken from [23].

interested reader to refer to the many available references [18][23].
Here we are mainly interested at the effect in terms of force that the atoms experience in a laser field so we report the result obtained for the *average* force[9] which is related only to the gradient of the atom-laser mode coupling:

$$\overrightarrow{f}(\overrightarrow{r}) = \langle b^{\dagger} a_L \nabla[\overrightarrow{d}\,\mathscr{E}_L] + b a_L^{\dagger} \nabla[\overrightarrow{d}\,\mathscr{E}_L^{q}]\rangle, \tag{2.19}$$

it is then possible to recover the well known equation:

$$\overrightarrow{f}(\overrightarrow{r}) = \frac{\hbar\Omega}{2} i\nabla\phi(\rho_{eg}e^{-i\phi} - \rho_{ge}e^{i\phi}) - \frac{\hbar\nabla\Omega}{2}(\rho_{eg}e^{-i\phi} - \rho_{ge}e^{i\phi}). \tag{2.20}$$

Here the terms $\rho_{eg} = \sum_n \langle e,n|\rho|g,n+1\rangle$ and $\rho_{ge} = \sum_n \langle g,n+1|\rho|e,n\rangle$ are the off diagonal terms of the density matrix of the states of the bare Hamiltonian.

The physical interpretation of the two terms in equation 2.20 is that the first part, proportional to the gradient of the phase $\phi(r)$, is the *radiation pressure* term while the second one, proportional to the gradient of the Rabi frequency Ω, is the

[9]Note that the results are still in the semiclassical approximation used before and the position operator is replaced by it's average value.

dipole force which we are mostly interested in.
To get a view of how the dipole force behaves it is useful to express it as a function of the populations and coherences of the dressed states:

$$\overrightarrow{f}_{dip} = \hbar\nabla\Omega'(\Pi_2 - \Pi_1) - \hbar\Omega'\nabla\theta(\rho_{12} + \rho_{21}). \tag{2.21}$$

Since the dipole force is related to the difference in the populations the effect is connected with the specific situation we are considering and the relative solution of the master equation for the density operator. The simplest case is the one for atoms at rest. It is important to notice that we are interested to cold atoms so that the atoms at rest situation is a good starting point and that the effects due to motion of the atoms[10] in the beam could be treated as corrections to this specific situation.

Dipole force for atom at rest

If the atom is at rest we can replace the populations with their steady state values Π_i^{st} and express the dipole force as a function of the forces experienced by the different dressed states $\nabla E_{1,2}$ as:

$$f_{dip}^{st} = -\Pi_1^{st}\nabla E_1 - \Pi_2^{st}\nabla E_2, \tag{2.22}$$

this is simply the mean between the two forces weighted by the probability of occupation. In terms of Rabi frequency and detuning it becomes:

$$f_{dip}^{st} = -\nabla\left(\frac{\hbar\delta}{2}\log(1+\frac{\Omega^2}{2\delta^2})\right). \tag{2.23}$$

Finally we can explain the connection between the sign of the dipole force and the sign of the detuning. Citing from [23]:

> We would like to show ow the dressed-atom approach gives a simple understanding of the connection between the sign of the dipole force and the sign of the detuning $\delta = \omega_L - \omega_a$ between the laser and the atomic frequencies. If the detuning is positive the levels 1

[10] These effects include, but are not limited to, Doppler shift and variation of the force over a wavelenght.

are those that coincide with $|g,n+1\rangle$ outside the laser beam. It follows that they are less contaminated by $|e,n\rangle$ than levels 2 and that fewer spontaneous transitions start from 1 than from 2. This shows that levels 1 are more populated than levels 2 ($\Pi_1^{st}\rangle\Pi_2^{st}$). The force resulting from levels 1 is therefore dominant, and the atom is expelled from high-intensity regions. If the detuning is negative, the conclusions are reversed: Levels 2 are more populated, and the atom is attracted toward high-intensity regions. Finally, if $\delta = 0$, both states 1 and 2 contain the same mixture of e and g, they are equally populated ($\Pi_1^{st} = \Pi_2^{st}$), and the mean dipole force vanishes.

This gives account for the two different possibilities to use the dipole force to cool atoms: blue detuned lasers ($\delta\rangle 0$) can be used to trap the atoms in the low intensity region of the beam whereas red dutuned one ($\delta\langle 0$) do the opposite. We will further discuss the concept of dipole trap in chapter 3.

Chapter 3

OPTICAL DIPOLE TRAPS

In this chapter we discuss the way to use the *dipole force* introduced in chapter 2 to trap, and eventually cool by evaporative cooling, atoms using a detuned laser.
We will mainly refer to the article of Grimm et al. of 1999 [27] and Philips of 1998 [45] in the this chapter.

3.1 Trapping atoms

3.1.1 Dipole potential: another approach

The optical dipole force arises form the interaction between induced atomic dipole moment and intensity gradient of the driving field ([27]). Here we report briefly the main results wich are useful for our work. The reader is urged to note that while the approach of the previous chapter was useful to introduce and understand the nature of the interactions giving rise to the dipole force and the radiation pressure from a quantum point of view, now it may be convenient to think of the dipole moment $\overrightarrow{p}$ in terms of the *complex polarizability* α and express its amplitude as

$$p = \alpha E, \tag{3.1}$$

where E is the amplitude of the electric field expressed in complex notation

$$\overrightarrow{E} = \hat{e}Ee^{-i\omega t} + c.c.$$

The interaction potential is therefore

$$U_{dip} = -\frac{1}{2}\langle \overrightarrow{p}\,\overrightarrow{E}\rangle_t = -\frac{1}{2\varepsilon_0 c}\Re(\alpha)I(\overrightarrow{r}), \tag{3.2}$$

where the angular brackets denote the time average over rapid oscillating terms and the intensity of the field is given by $I = 2\varepsilon_0 c|E|^2$.

The polarizability is a function of the damping rate Γ (corresponding to the spontaneus decay rate from the excited level)[27]:

$$\alpha = 6\pi\varepsilon_0 c^3 \frac{\Gamma/\omega_0}{\omega_0^2 - \omega^2 - i(\omega^3/\omega_0^2)\Gamma}. \tag{3.3}$$

The calculation of Γ may be done in a classical way using the Larmor formula, in a semiclassical approximation (two level atoms + classical radiation) or even in a fully quantized approach. For most purposes with alkali atoms using the classical formula $\Gamma = \frac{e^2\omega^2}{6\pi\varepsilon_0 m_e c^3}$ is enough, but for coherence with the previous chapter we express it in the semiclassical approximation:

$$\Gamma = \frac{\omega_0^3}{3\pi\varepsilon_0\hbar c^3}|\langle e|\hat{d}|g\rangle|^2. \tag{3.4}$$

In the usual RWA and in the limit of large detuning and negligible saturation (the excited level is far from being fully occupied) the expression for the dipole potential is derived as:

$$U_{dip} = \frac{3\pi c^2}{2\omega_0^3}\frac{\Gamma}{\delta}I(\overrightarrow{r}) \tag{3.5}$$

and the scattering rate may be expressed as:

$$\Gamma_{sc} = \frac{3\pi c^2}{2\hbar\omega_0^3}(\frac{\Gamma}{\delta})^2 I(\overrightarrow{r}). \tag{3.6}$$

Even in this semiclassical approximation we have recovered the dependance of the potential (and therefore of the force) on the sign of the detuning δ. It may be useful to express the scattering rate as a function of the dipole potential:

$$\Gamma_{sc} = \frac{\Gamma}{\delta}U_{dip},$$

therefore a large detuning is often used to reduce the scattering rate keeping the depth of the trap constant.

3.1.2 Alkali atoms

Many experiments in atom cooling are done with alkali atoms. This is due to their rich internal structure that on one side blurs the simple 'two-level system' picture, on the other offers plenty of opportunities for deeper investigation and sub-doppler cooling [43],[45] and [7]. At the BIARO experiment (see chapter 4) Rubidium atoms (^{87}Rb) are used.
The $ns \rightarrow np$ transition, for a nuclear spin $I = \frac{3}{2}$, has a complex scheme due to fine splitting Δ_{FS} and hyperfine splitting Δ_{HFS} for each level (see fig: A.2). Let's remind that the energy scale is $\hbar\Delta'_{FS} \gg \hbar\Delta_{HFS} \gg \hbar\Delta'_{HFS}$, where the prime refers to the excited state.

For unresolved hyperfine splitting of the excited level (i.e. all optical detunings $\delta \gg \Delta_{HFS}$), the *ground state* of an atom with total angular momentum F and magnetic quantum number m_F 'feels' a light polarization potential [27]:

$$U_{dip}(r) = \frac{\pi c^2 \Gamma}{2\omega_0^3} \left(\frac{2 + \mathscr{P} g_F m_F}{\delta_{2,F}} + \frac{1 - \mathscr{P} g_F m_F}{\delta_{1,F}} \right) I(r). \tag{3.7}$$

Here g_F is the Landé factor, $\mathscr{P}$ refers to the polarization of the light ($\mathscr{P} = 0, \pm 1$, for linearly and circularly $\sigma^{\pm}$ polarized light) and the detunings $\delta_{1/2,F}$ refer to the energy splitting between the ground state $^2S_{1/2}, F$ and the center of the hyperfine split of the the excited levels $^2P_{3/2}$ and $^2P_{1/2}$ respectively.

3.1.3 Blue-detuned and red-detuned dipole traps

We have seen in sections 2.2.2 and 3.1.1 that the sign of the dipole force and potential (as well as lightshift of the energy levels) depends on the sign of the detuning δ. Traps realized with $\delta > \omega_a$ are called *red-detuned dipole traps* while the ones realized with $\delta < \omega_a$ are called *blue-detuned dipole traps*.
The main difference is that red detuning provides a minimum of the potential in the high laser intensity region (e.g. the focus of the laser beam) whereas blue detuned light 'repels' the atoms toward regions of low intensity (see Figure 3.1).

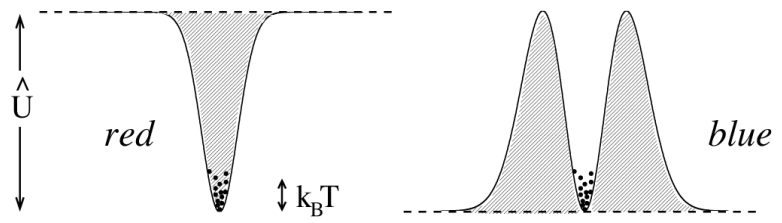

Figure 3.1: Dipole traps with red (left) and blue (right) detuning. For the red-detuned trap a Gaussian profile is assumed for the laser beam whereas a Laguerre-Gaussian LG_{01} mode is taken for the blue-detuned one. Image taken from [27].

Red-detuned optical dipole traps

As stated in previous sections for a red detuning the focus of a laser beam provides the first example of a stable dipole trap; in fact it is the simplest one, but there are other possible solutions (see Figue: 3.2), like *standing wave traps* (that are useful to realize a 1D lattice of shallow potential minima) and *crossed-beam traps* on which we will focus more. Crossed-beam traps are used to resolve the anisotropy of the confinement that in a single laser beam trap is strong in the transverse direction and weak in the propagation direction.

It should be noted that with red detuned focused beam traps the attainable trap depth is of the order of *mK*, much smaller than thermal energy of the room temperature atoms: it is therefore *necessary* to pre-cool the atoms before being able to load them in such a trap.
Tipically the traps are loaded from pre-cooled atoms trapped in a magneto-optical trap (MOT); the specific configuration of the MOT(s) and their position with respect to the dipole trap depend on the purpose and on the creativity of the experimenters. We will briefly describe the configuration of the BIARO experiment in section 4.1.
After loading a crossed-beam trap it is possible to use it to perform evaporative cooling (see [1] for a 'proof of principle' experiment with *Na* atoms), a technique that is fundamental to increase phase-space density, that has been the key to obtain Bose-Einstein condensates [4], [24]. In order to achieve evaporative cooling the

optical power of the laser used for the trap is ramped down to allow the atoms with higher thermal energy to escape from the trap. After thermalization of the atoms remaining in the trap, the temperature is decreased and the phase-space density may increase.

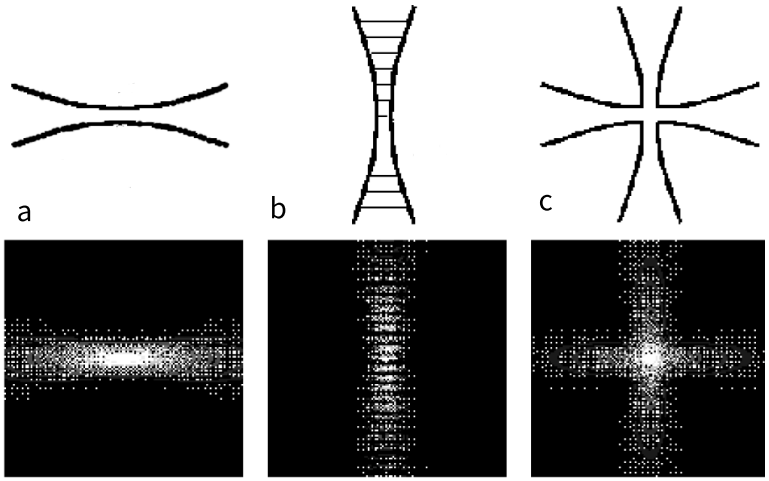

Figure 3.2: Dipole traps types. a) Single focused beam trap. b) Standindg wave trap. c) Crossed beam trap. Image taken from [27].

Blue-detuned optical dipole traps

Blue-detuned light offers the possibility to realize traps in which the atoms are stored in a *'dark'* spot, therefore reducing the effects of light on the sample atoms. In particular there is no or little light shift of the energy levels, photon scattering is greatly reduced and losses due to interaction with light are limited.
There are however some disadvantages in realizing these kind of traps, mainly due to the fact that the laser beam repels the atoms and is necessary to realize 'walls' around the dark area in which the sample is to be confined.
The balance of these two aspects makes blue-detuned dipole traps efficient in the situation of hard repulsive optical walls or large potential depth for tight confining ($U \gg k_B T$). For an extensive description of the possible geometries and means to

realize a trap using blue detuned light refer to [27] or [43].

3.2 Cooling methods in dipole traps

In this section we briefly review the most used methods for cooling samples in dipole traps. We remind, for historical reasons, that atom cooling methods have been enhanced greatly in the late eighties and in the nineties of the 20th century and that the field is still growing, though at a slower pace.
The first big step has been the developement of *Doppler cooling*: this method is "based on cycles of near resonant absorbtion of a photon and subsequent spontaneus emission resulting in a net atomic momentum change per cycle of one photon momentum $\hbar k$ with $k = 2\pi/\lambda$ denoting the wave number of the absorbed photon"[27]. Since spontaneus emission give rise to heating due to momentum recoil, the limit in reacheable temperature is given by the equilibrium between heating and cooling. Theoretical treatment of Doppler cooling relies on the simple two-level atom picture. The minimum temperature reacheable with this method is called *Doppler temperature* $k_B T_D = \hbar\Gamma/2$ and is of the order of $10^{1-2} mK$, just enough to load a dipole trap.
To reach sub-Doppler temperatures one has to exploit the complex structure beyond the two-level picture; *polarization gradient cooling* is realized with standing waves with spatially varying polarization and relies on optical pumping between Zeeman sublevels of the ground state. The most-famous version of this method is probably the "Sysiphus cooling" [23] in which an atom loses kinetic energy climbing up the dipole potential induced by a standing wave with varying polarization; when the polarization of the wave changes from σ^+ to σ^- the light shift of two Zeeman sublevels must change in a correlated way in order to make a moving atom runs up a potential hill more often than it runs down. The net effect is that the loss in kinetic energy is greater than the gain. For a comprehensive description and illustration of this method see [19] or [45]. Exploiting Sysiphus effect allows to reach temperatures of the order of $10T_{rec}$ where the recoil temperature, defined

as

$$T_{rec} = \hbar^2 k^2 / m, \tag{3.8}$$

is the gain in temperature associated with the kinetic energy gain due to the emission of one photon. For alkali atoms T_{rec} is of the order of the μK, being equal to $0.36\mu K$ for Rubidium 87 that is used in the BIARO experiment.

To reach sub-recoil temperatures one has to introduce an absorbing mechanism that is sensible to atom velocity; the idea is to make the atoms with velocity close to zero dark to the absorbtion-emission mechanism. *Raman* cooling [33] is realized with Raman pulses from two counterpropagating lasers that transfers atoms between two ground levels $|g_1\rangle$ and $|g_2\rangle$ transferring $2\hbar k$ momentum in each absorbtion. Adjusting frequency width, detuning and propagation direction one can tailor pulses that excite all atoms but the one with velocity close to zero. Spontaneus emission from excited atoms in $|g_2\rangle$, being random in direction, brings atoms back to $|g_1\rangle$ leaving a bigger fraction of the sample with (almost) zero velocity. Repeating the cycle allows to accumulate atoms in a small velocity interval around $v = 0$ thus cooling the sample. Raman cooling allows to reach sub-microkelvin temperature but requires pre-cooling with another mechanism being effective on samples with starting temperature of the order of few tens of microkelvin.

Resolved-sideband Raman cooling

Resolved-sideband Raman cooling is a tecnique developed first for laser cooling in ion traps and later adjusted for trapping neutral atoms [57]. The requirement for this method of cooling is to have a strong confinement of the atoms in at least one dimension, with oscillation frequency ω_{osc} large enough to be resolved by inelastic Raman transitions between two ground levels. The degeneracy of the ground level is usually resolved with the aid of a small magnetic field, therefore the splitting between the ground levels is of the order of a Zeeman splitting.
The atomic motion is described by a wavepacket formed of a superposition of vibrational states $|v\rangle$; in the Lamb-Dicke regime (rms size of the wavepacket small compared with the wavelenght of the cooling transition) almost all absorbtion-

spontaneous emission cycles returns to the same vibrational state ($\Delta\nu = 0$). To perform resolved-sideband Raman cooling one must repeat cycles of Raman pulses tuned to excite transitions with $\Delta\nu = -1$ followed by optical pumping into the initial state with $\Delta\nu = 0$. The net effect the motional ground state $|\nu = 0\rangle$ is selectively populated since it is the only state that is dark to the Raman pulses.

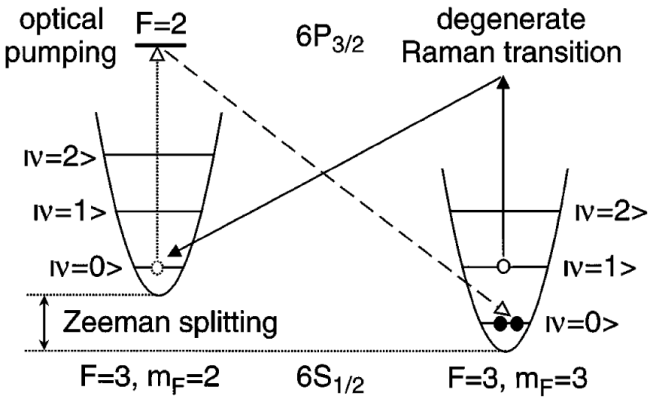

Figure 3.3: Resolved-sideband cooling scheme using the two lowest ground states of *Cs* atoms. Image taken from [57].

Chapter 4

THE BIARO EXPERIMENT

In this chapter we will describe the experimental setup and the purpose of the BIARO experiment. In section 4.1 we will give a brief description of the apparatus, the cavity and the cooling methods used in the experiment. In the subsequent section, 4.2 we will introduce Bose Einstein condensation and describe how it has been possible to reach it in the BIARO experiment. Section 4.3 is devoted to how to perform a QND measurement in the experiment; from the theoretical analysis of such measurements it has been predicted the possibility to produce non classical atomic states using QND measurements [54]. These kind of measurements have been recently used to perform feedback which is a mean to fight naturally occurring decoherence of a coherent spin state[55].
Section 4.4 is a brief discussion of the compensation of the differential light shift induced by the trapping radiation on the levels involved in the D2 transition.

The setup, the theoretical analysis and all the experimental results reported in this chapter have been realized in the years from 2009 by the scientists that have worked on it until now. The description of the state of the experiment is important to understand the purpose of the work described in chapter 5.

4.1 Experimental setup

In this section we will describe the setup: the cavity, the trapping and the cooling methods.

The experimental apparatus is composed of two chambers: the first is kept under high vacuum (pressure below 7×10^{-8}mbar) and a 2 dimensional magneto-optical trap (MOT) is operated and used as a source[1] of pre-cooled atoms. The science chamber is kept under ultra-high vacuum (pressure below 10^{-9}mbar) and contains the coils for a 3D MOT as well as the crossed optical cavity. Experiments are realized in the science chamber at the center of the cavity.
Technical details on this part may be found in [8] [9] [10] [37] [53] [54] [55].

4.1.1 The high finesse cavity

Here we report a description of the main properties of the cavity; the full characterization of the cavity is reported in [8] and [52]
The cavity is in a butterfly configuration (see fig 4.1), an ingenious idea to provide high trapping (i.e. deep potential) with low power laser. The geometry of the cavity allows the realization of a crossed-beam dipole trap (see section 3.1.3 and Fig: 3.2).

The cavity is made up of four mirrors placed at the corners of a square with a diagonal of 90mm; two mirror mounts are completely fixed while one is actuated by piezoelectric actuators, which allow for a coarse alignment of the cavity. The last mount is a piezo-actuated three-axis nano-positioning system with a maximal angular displacement of 2mrad and a translation of 50μm. It is used to finely adjust the cavity crossing angle and dynamically control the cavity length [8]. The four mirrors of the cavity are highly reflecting at both 1560nm and 780nm. The free spectral range (FSR) of the cavity is 976.2MHz and the cavity's full width at half maximum (FWHM) linewidth is $\gamma = 546kHz$ at 1560 nm.

The finesse[2] of the cavity has been studied *a priori* for the two resonating wave-

[1] The source of atomic background pressure is the vapor pressure of a 1g ^{87}Rb sample.

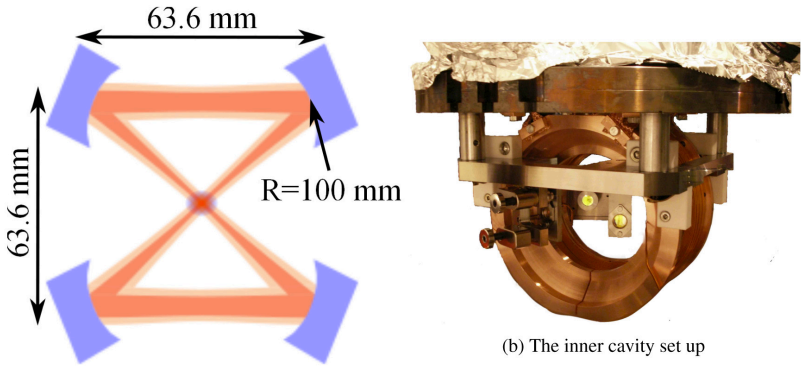

(a) Scheme of the cavity geometry

(b) The inner cavity set up

Figure 4.1: a)Scheme of the butterfly cavity.b)The inner vacuum setup with the suspended cavity and the coils generating the MOT magnetic field; image taken from [9]

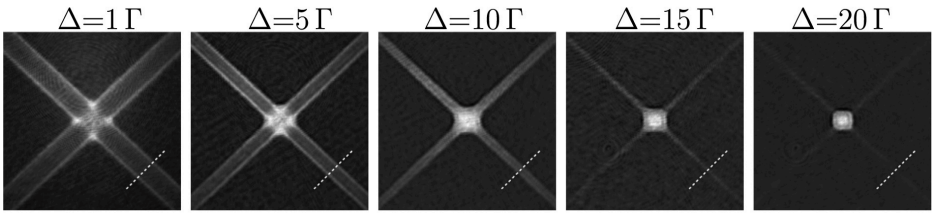

Figure 4.2: Tomographic images of the optical potential. The images are obtained setting the probe frequency to different detuning Δ with respect of the D_2 line. The images represent atoms with energy levels lightshifted in a position-dependent manner. Atoms which are sensitive to higher detuning are experiencing a higher lightshift *i.e.* they are deeper in the optical potential. Image taken from [9].

lenghts and then measured [9] for 1560nm obtaining $\mathscr{F}_{1560} = 1788$.
The trapping laser radiation at 1560*nm* is injected in the cavity and excites the fundamental transverse electromagnetic (TEM00) mode: both the magnetic and the electric field are perpendicular to the direction of propagation[3]. Tomographic images of the optical potential have been obtained with *light-shift tomography* [15]. The 1560*nm* laser has been locked to the cavity using a Pound-Drever-Hall technique [25] that allows to fast correct the frequency with an acousto-optic modulator in double pass [8] [9]. Frequency stabilization of the trapping radiation has been improved using *serrodyne modulation* as described in [37]. The 780*nm* probing radiation is obtained by doubling the frequency of the trapping laser.

Higher modes of the cavity

The use of phase masks allows an efficient injection of modes of the cavity different from the fundamental TEM00. In particular in [10] there is the full description of the method used to lock the 1560*nm* laser to the TEM10 and TEM20 modes. These modes may be used in the future to trap atoms in a well defined lattice, cool the atoms down to the BEC temperature (see section 4.2) and obtain a lattice of BECs. This geometry can be superimposed to the fundamental mode of the cavity during an experimental sequence: therefore it may be used to split the condensate trapped in the fundamental mode and perform experiments on condensates in each lattice site and then regroup the condensate by removing the higher modes. It may be possible in the future to exploit this feature to perform high precision atomic interferometry using the BECs [8].

4.1.2 The trapping

The Gaussian profile of the 1560*nm* beam that excites the fundamental mode of the cavity produces a position dependent lightshift on the levels of our interest,

[2]The finesse F of the resonator is defined as the ratio of the FSR and the FWHM of a resonance for a specific resonance wavelength.

[3]See, for instance, [36] or R. Paschotta *Encyclopedia for Photonics and Laser Technology*, Wiley-VCH in the open access online version available at *rpp-enc.com*.

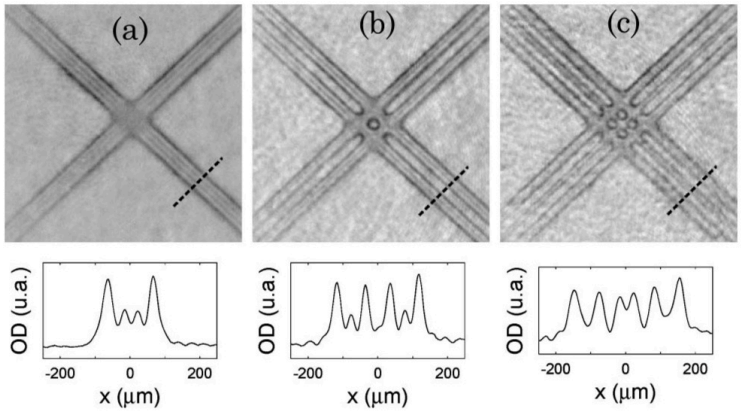

Figure 4.3: . Image taken from [9].

that realize an optical dipole trap. Considering only the relevant D_1 and D_2 transitions, the ground level $5S_{1/2}$ is downshifted for a maximum of the intensity so atoms will be trapped in the ground state at the center of the Gaussian beam. The $5P_{3/2}$ state would be, if we consider only the D lines, blue-shifted and would expel the atoms at the maximum of the intensity. Since the $5P_{3/2} \rightarrow 4D_{5/2,3/2}$ transitions are at $1529nm$ it is important to take them into account; for these transitions the trapping radiation is red-detuned so the $5P_{3/2}$ level is red-shifted; the proximity of these $1529nm$ resonances makes the light shift on the $5P_{3/2}$ level large compared to the one of the ground state resulting in a *differential light-shift* of the relevant level as shown in Fig: 4.4. The trapping of the atoms is done in three steps: using the 2D MOT an array of cold atoms it is realized and eventually directed towards the 3D MOT [52]. The array of cold atoms is then trapped in a 3D MOT centered on the cavity crossing region (and $3mm$ above the 2D MOT jet to avoid direct collisions with thermal atoms). In this situation it is possible to obtain an atomic cloud of a few 10^9 atoms after 3 seconds of loading [9].
The last step, described in [9], is the transfer of the atoms from the 3D MOT to the dipole trap realized with the trapping radiation at $1560nm$.
After the loading sequence about 25×10^6 atoms are trapped at the crossing region of the dipole trap at a temperature $T = 230\mu K$. The number of atoms in

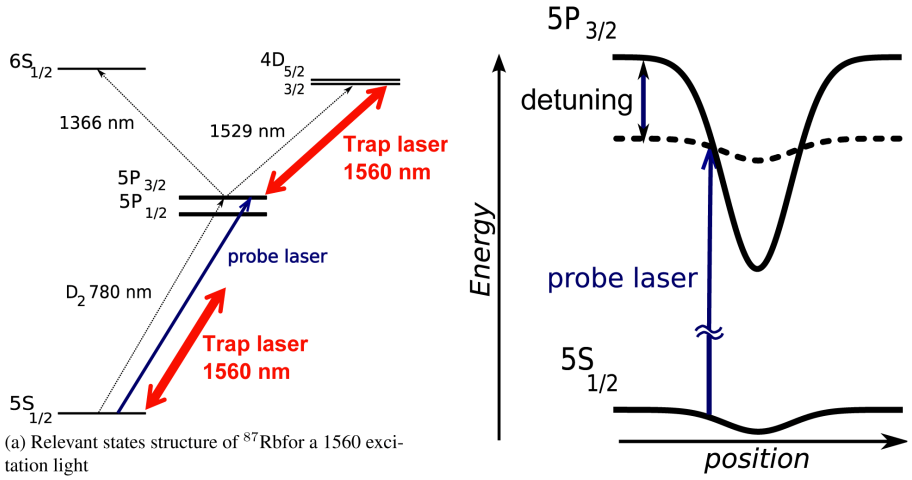

(a) Relevant states structure of ^{87}Rbfor a 1560 excitation light

(b) Differential light-shift of the imaging transition

Figure 4.4: . Image taken from [8].

the trap decreases with exponential behaviour (lifetime $\tau = 6.7s$); the temperature was measured to be constat in the dipole trap, meaning that the trap itself do not heat the atomic sample: the heat is exactly compensated by the energy lost trough evaporation of the most energetic atoms.

4.1.3 Cooling

The optical cooling of the atomic sample requires two lasers. The first one is tuned of about 3Γ on the red side of the cycling transition $|F = 2\rangle \rightarrow |F' = 3\rangle$; the photon is absorbed with higher probability from the direction against velocity of the atom. The momentum transfer gives a *kick* in the opposite direction slowing down the atom. Since there is non zero probability to excite the transition $|F = 2\rangle \rightarrow |F' = 2\rangle$ and since from $|F' = 2\rangle$ the atoms can decay to the ground level $|F = 1\rangle$ which is dark to the cooling laser, a *repumper* tuned on the transition $|F = 1\rangle \rightarrow |F' = 2\rangle$ that repumps the atom on the $|F = 2\rangle$ level is used [8] [53]. The two lasers are extended cavity laser diode: the repumper is locked to the hyperfine $|F = 1\rangle \rightarrow |F' = 2\rangle$ transition through frequency modulation spectroscopy

and the cooling laser is frequency locked to the repumper. The frequency of the cooling laser may be changed with respect to the atomic transition and this is essential to load the optical dipole trap from the MOT. The two lasers used for the cooling are injected in a fiber cable and used both for the 2D and the 3D MOTs [8], [9], [53].

Evaporative cooling

To obtain Bose Einstein condensation (see section 4.2) in the dipole trap, evaporative cooling is used. The quantum degenerate regime for the BEC requires small interatomic spacing in the sample which is obtained with high trapping frequency. It is then important to measure the frequencies of the trap to define an optimal ramp for the evaporative cooling: the chosen ramp must result in increased phase space density of the sample. A theoretical analysis of the frequencies of the trap is reported in [8] and [53].

Measuringthe trap frequencies

It is worth citing two experimental methods to measure the trap frequencies: the first exploits *parametric heating* whereas the second measures the modes of oscillation after a sudden change of the geometry of the trap [53].
To measure the trapping frequencies exploiting parametric heating a sinusoidal modulation is applied on the trapping depth after loading the trap. After a fixed number of oscillation (500 in the context of BIARO) the number of atoms at the center of the trap is measured. Sweeping over a range of frequencies it is possible to find the resonance frequency, characterized by important losses in the number of atoms. In parametric heating the resonance frequency is twice of the frequency of the system (in our case of the trap). The horizontal frequency $\omega_x = \omega_y$ is found to be equal to $700Hz$ when the intra-cavity power is $240W$ [53].
When the frequency is measured by changing the shape of the trap, the idea is to suddenly increase the intra-cavity power (up to $240W$ in the context of BIARO) and observe the oscillation of the size of the atomic cloud: the frequency of this

oscillation is, if one takes the image from a direction wich is perpendicular to the arms of the cavity, double of the frequency of the trap. This method confirmed the results of parametric heating allowing an estimate of $\omega_{x,y} = 600Hz$ [53].

4.2 Bose Einstein condensates

We know from statistical mechanics [5][32] that a boson gas at finite temperature may display *macroscopic* population of the ground state. This striking feature is signature of a state of matter called *Bose Einstein condensate* (BEC).
In quantum mechanics particles are described by wavefunctions with a spatial extent given by the de Broglie wavelenght $\lambda = h/p$ that, in the case of a gas of identical particles at a temperature T becomes the so called *thermal de Broglie wavelenght*:

$$\lambda_{DB} = \frac{h}{\sqrt{2\pi m k_B T}}, \tag{4.1}$$

where m is the mass of the particles composing the gas and k_B is the Boltzmann constant. When particles in a gas are so close to each other that their wavefunction overlaps constructive interference may occur. Particles become no longer distinguishable from each other and the system crosses the critical point of Bose Einstein condensation. It is possible to define the density in phase space

$$D = n\lambda_{DB}^3, \tag{4.2}$$

where n represents the density of the atoms in terms of particles per unit volume, and distinguish two regimes for $D \ll 1$ and $D \approx 1$. The first regime represents a gas where the interatomic spacing is much greater than the de Broglie wavelength and where the wave character of the particles is of little interest; in such a regime the particles follow the Maxwell-Boltzmann distribution: we call this the classical regime or refer to this as a classical gas. When the phase-space density increases and reaches $D \approx 1$ the wave nature of the particles becomes relevant and it is possible to reach the transition to BEC, where the system (or a macroscopic fraction of the system) is described as a coherent wave of matter.
If the particles are trapped in a harmonic trap, such as an optical dipole trap, it is

possible to describe the appearence of this latter state of matter in terms of saturation of the excited states. Following [8], we consider a 3D harmonic trap in the form:

$$V(\overrightarrow{r}) = \frac{1}{2}m(\omega_x^2 x^2 + \omega_y^2 y^2 + \omega_z^2 z^)), \tag{4.3}$$

where ω_i represent the trapping frequencies, and the potential admits a discrete set of energy levels:

$$\varepsilon_{n,m,p} = \hbar(n\omega_x + m\omega_y + p\omega_z). \tag{4.4}$$

If we have N bosons in the trap at a temperature T, the number of particles in each level follows the Bose Einstein distribution:

$$N(\varepsilon_{n,m,p}) = \frac{1}{e^{\frac{\varepsilon_{n,m,p}-\mu}{k_B T}} - 1}. \tag{4.5}$$

The number of particles in the excited states, for a harmonic trap, is limited to [22]:

$$\sum_{n,m,p\neq 0} N(\varepsilon_{n,m,p}) = \zeta(3)\left(\frac{k_B T}{\hbar\omega_m}\right), \tag{4.6}$$

where $\zeta(n)$ is the Riemann function and $\omega_m = (\omega_x\omega_y\omega_z)^{1/3}$ is the average of the trapping frequencies. The number of particles in the ground state may be expressed as:

$$N_0 = N - \sum_{n,m,p\neq 0} N(\varepsilon_{n,m,p}), \tag{4.7}$$

from which it is evident that if the total number of particles is increased above the saturation value of eq. 4.6, the atoms have to accumulate in the ground state of the harmonic oscillator.

It is possible to express the critical temperature T_c for the apparition of such behavior as a function of the number of atoms N:

$$T_c = \frac{\hbar\omega_m}{k_B}\left(\frac{N}{\zeta(3)}\right)^{1/3} = 0.94\frac{\hbar\omega_m}{k_B}N^{1/3}. \tag{4.8}$$

It becomes clear that high trap frequencies are related to high critical temperature.

Bimodal distribution of the density

The atoms in the ground state of a harmonic potential are described by a wavefunction

$$\phi_0(\overrightarrow{r}) = \left(\frac{m\omega_m}{\pi\hbar}\right)^{3/4} e^{\frac{-m}{2\hbar}(\omega_x x^2+\omega_y y^2+\omega_z z^2)}, \tag{4.9}$$

resulting in a density of the condensate that is $n(\overrightarrow{r}) = N|\phi_0(\overrightarrow{r})|^2$ and an extension of the ground state

$$a_{ho} = \left(\frac{\hbar}{m\omega_m}\right)^{1/2}.$$

On the other hand the atomic density of the thermal part (excited states) follows a Maxwell-Boltzmann distribution $n(\overrightarrow{r}) = n_0 e^{-V(\overrightarrow{r})/k_B T}$ with a width

$$\sigma = \left(\frac{k_B T}{m\omega_m}\right)^{1/2}.$$

The appearence of a superposition of this two distributions, what is called a *bimodal distribution*, in the density distribution of the atoms in the trap at a temperature below T_c is then a signature of the presence of a fraction of atoms in the condensed state.

4.2.1 Effect of the interactions

In the previous section we neglected, on purpose, the effect of interactions treating the gas as non-interacting. To determine the extension of the wavefunction and the atomic density in a real gas the effect of interactions must be taken into account. In the case of a dilute gas, where the scattering length a is small compared to interatomic distance $n^{-1/3}$ it is possible to treat the effect of the interactions in a mean field theory [5][22] that gives rise to an effective repulsive field in the form $V_{rep} = g_{rep} n(\overrightarrow{r},t) = g_{rep}|\psi(\overrightarrow{r},t)|^2$ where $g_{rep} = 4\pi\hbar a/m$. The evolution of the wavefunction is then given by the *Gross-Pitaevskii equation*:

$$i\hbar\frac{\partial}{\partial t}\psi(\overrightarrow{r},t) = \left(-\frac{\hbar\nabla^2}{2m} + V_{ext}(\overrightarrow{r}) + g_{rep}|\psi(\overrightarrow{r},t)|^2\right)\psi(\overrightarrow{r},t). \tag{4.10}$$

If we look for the ground state the problem is time indipendent and the wavefunction can be separated in $\psi(\overrightarrow{r},t) = e^{-i\frac{\mu}{\hbar}}\varphi(\overrightarrow{r})$ where the amplitude of density

$\varphi(\overrightarrow{r})$ verifies

$$\mu\varphi(\overrightarrow{r}) = \left(-\frac{\hbar\nabla^2}{2m} + V_{ext}(\overrightarrow{r}) + g_{rep}|\varphi(\overrightarrow{r})|^2\right)\varphi(\overrightarrow{r}), \tag{4.11}$$

and the chemical potential μ represents the energy cost to take one atom out of the condensate.

If the density $n_0(\overrightarrow{r}) = |\varphi(\overrightarrow{r})|^2$ presents a slow spatial variation the kinetic energy term becomes small compared to the interaction energy and may be neglected. This is the *Thomas-Fermi regime*[22], where eq. 4.10 has an analitical solution and the density becomes:

$$n_0(\overrightarrow{r}) = max\left\{\frac{\mu - V_{ext}(\overrightarrow{r})}{g_{rep}}, 0\right\}. \tag{4.12}$$

The wavefunction takes then the shape of the trapping potential that is, in the case of a harmonic potential, a reversed parabola. It is possible to define the Thomas-Fermi radius of the parabola through the point where the density becomes zero:

$$R_{TF} = \sqrt{\frac{2\mu}{\hbar\omega_m}}. \tag{4.13}$$

The density at the center of the condensate is limited by the interactions and in the Thomas-Fermi approximation is given by $n_0 = \mu/g_{rep}$.

The interactions not only affect the wavefunction of the condensate but also the transition from the thermal gas. Repulsive interaction results in the appearence of the BEC at a temperature $T < T_c$. The fraction of condensed atoms evolves with temperature following:

$$\frac{N_0}{N} = 1 - \left(\frac{T}{T_c}\right)^3 - \eta\frac{\zeta(2)}{\zeta(3)}\left(\frac{T}{T_c}\right)^2\left[1 - \left(\frac{T}{T_c}\right)^3\right]^{2/5}, \tag{4.14}$$

where η is an adimensional parameter that characterizes the thermodynamics of the boson gas in the trap [22].

4.2.2 BEC in the frame of BIARO experiment

With the experimental setup described in section 4.1 BEC has been attained in 2011 through evaporative cooling in the optical dipole trap. Here we report the

main steps to reach the degenerate regime in the BIARO experiment.
The density in phase-space in the dipole trap evolves following

$$D = N\left(\frac{\hbar\omega_m}{k_B T}\right)^3 \tag{4.15}$$

and to reach BEC it has to become of the order of unity. To reach such a high density in phase-space it is necessary to lower the temperature while keeping a high mean trapping frequency and a high number of atoms in the trap. A high mean trapping frequency it is required to have a high scattering rate for the atoms in the trap, hence fast thermalization.
Starting parameters after trapping the atoms in the dipole trap are $T \approx 250\mu K$, $\omega_m = 2\pi \times 790Hz$ and $N \approx 10^8$ resulting in $D \approx 3.5 \times 10^{-4}$.
Evaporative cooling allows to lower T but reduces ω_m and N as well as the collision rate that is necessary to allow rethermalization of the sample after each stop of the cooling ramp. To perform it in a dipole trap it is sufficient to reduce the intra-cavity power. Adjusting the cooling ramp [53] allows to reach a density $D \approx 10^{-2}$ with a final number of atoms $N \approx 10^7$. With a number of atoms less than 10^7 the phase-space density does not increase since the effect of gravity becomes relevant and modifies the trapping potential: further evaporation causes a decrease of the trapping frequency which is too fast.
To overcome this limit a vertical beam, orthogonal to the trapping beams, with the focus on the trap has been added (see Fig: 4.5). This beam forms a *dimple* that allows to evaporate atoms without decreasing the horizontal trapping frequencies. The dimple provides strong transverse confinement, with horizontal trapping frequencies measured to be $\omega_x = \omega_y = 2\pi \times 550Hz$, and an escape on the vertical direction. The optical power of the dimple is about $200mW$.
It is now possible to lower the depth of the trap to further cool the sample. The mean frequency being now $\omega_m \approx 2\pi 250Hz$, the remaining number of atoms $N \approx 5^4$and the temperature $T \approx 200nK$ realizing $D \approx 4.3$, a value for which Bose Einstein condesation is expected. Signature of the transition have been found observing a bimodal distribution of the density measured through the *time of flight method* [53]. Results are reported in Fig: 4.6

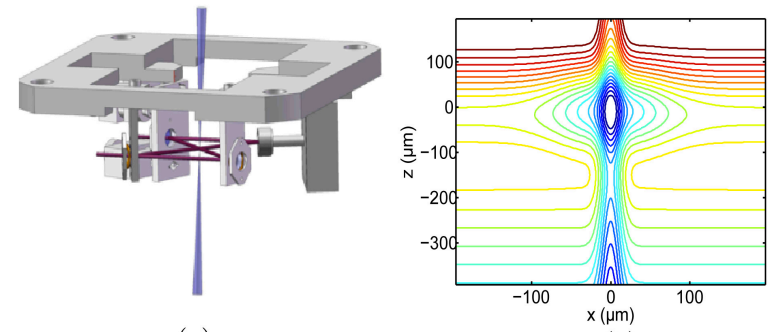

Figure 4.5: Dimple. a) Position and alignment of the dimple. b) Isopotentials of the dipolar potential obtained superposing the fundamental mode of the cavity and the dimple. Image taken from [53]

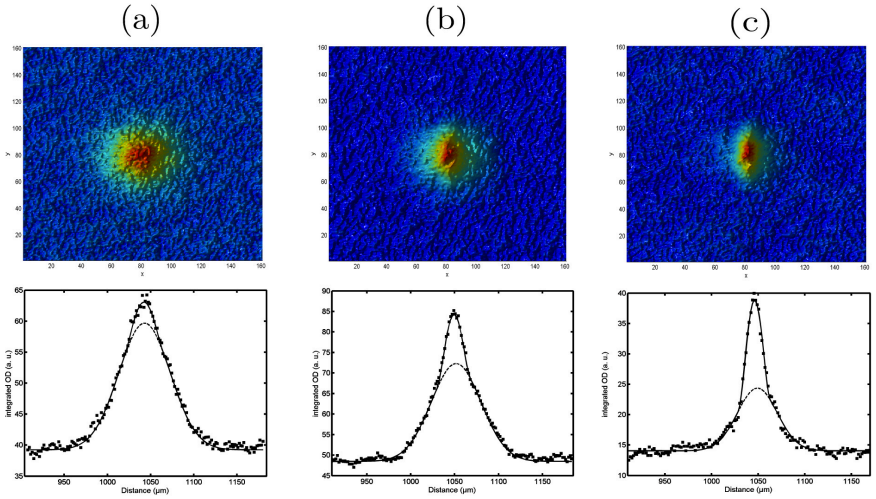

Figure 4.6: Bimodal distribution of the density, signature of the presence of a fraction of the sample in the condensed state. First row: optical density after a time of flight of $8ms$. Second row: optical density integrated on the vertical direction; the condensate part has been fitted with an inversed parabola, the thermal part with a Gaussian. a)$T = 0.8T_c$ $(145nK)$ b)$T = 0.7T_c$ $(131nK)$ c)$T = 0.4T_c$ $(74nK)$. Image taken from [53].

4.3 Quantum state engeneering techniques

In this section we report the analisys, made in [8][54], of the theoretical model that should allow the realization of spin squeezed states (SSS) and Dicke states through QND measurements. Quantum state engineering techniques are developed to maximize the sensitivity of measurement devices [9], a feature of main importance in quantum metrology. Entangled states like SSS may be used to overcome the standard quantum limit (see section 1.3.3) given by the atomic shot noise [9]. Generation of such states through heterodyne non-destructive measurement of the atomic population is expect and needs to be further investigated[54]. Using a scheme based on the frequency modulation spectroscopy allows to be limited to the shot noise of a weak optical probe; frequency modulation and heterodyne detection allows the rejection of even small path length fluctuations which are critical for the detection of small phase shifts [9].
It has been also possible to perform feedback to fight the loss of coherence induced by ambient noise [55]: an ensemble of Rubidium atoms is prepared first in a coherent superposition of the two ground hyperfine levels $|F = 1, m_F = 0\rangle$ and $|F = 2, m_F = 0\rangle$ of the electronic ground state $5^2S_{1/2}$, then is subjected to a collective noise obtained manipulating the ensemble with a microwave pulse that evolves the collective spin state. The direction of the collective noise is established whereas the sign is generated by a quantum random number generator. Finally the population difference is *weakly* measured using an optical probe; the information from the measurement is used to evalute the effect of the noise and a microwave pulse in the opposite direction is used to complete the feedback loop.

4.3.1 Realization of SSS and Dicke states

A theoretical analysis of the measurement process predicts that it is be possible to realize spin squeezed states and Dicke states. At the time of the writing of this thesis the experimental realization has failed to produce such states.
The frequency modulation (FM) spectroscopy technique is used: a laser beam is phase modulated to produce frequency sidebands, one of wich is placed close

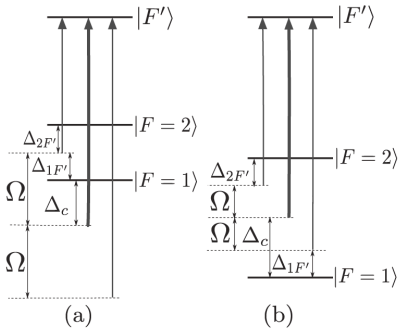

Figure 4.7: Two possible measurement schemes. The thick line is the carrier while the thin lines are the sidebands. a) One sideband is in the middle of two probed states whereas the carrier and the other sideband are far from the relevant transition. The population of the upper level is probed. b) Each sideband is close to an atomic transition; the carrier is in the middle of the two probed states; this configuration allows the direct measurement of the population difference J_z. Image taken from [54]

to an atomic transition and experiences a strong phase shift passing through the atomic sample while the carrier is far detuned from every transition, therefore passes through the sample without experiencing phase shift. The detection of the beat note at the modulation frequency allows to estimate the atomic population of the probed state.
The relevant atomic levels and the position of the carrier and sidebands in two possible configurations is depicted in Fig: 4.7.

The starting atomic state is a CSS polarized along J_x, wich means an average population difference $\langle J_z \rangle = 0$. The input optical state is composed of two spectral modes: the probe at a frequency $\omega_0/2\pi$ is close to an atomic transition whereas the reference is far off resonance at a frequency $(\omega_0+\Omega)/2\pi$; "a single-sideband optical phase modulator B (driven by a local oscillator at a frequency $\Omega/2\pi$) is used as a spectral beamsplitter to generate spectrally mode-entangled single photons" [54].

A theoretical analysis of the measurement process is realized in [54] and shows

that the back-action of the QND measurement in the weak coupling regime allows for the preparation of SSS in the *short time limit* whereas in the *long time limit* preparation of Dicke states is achieved.
The short time limit is defined by $N_P \ll M^{-2}$ where N_P represents the number of photons detected and M is a measure strenght defined as

$$M^2 = \frac{\phi^2}{4}(1-\sqrt{1-C^2}); \tag{4.16}$$

here ϕ is the optical phase shift induced by a number difference of two ($n = 1$), and depends on the coupling strength of the transition at ω_0 and on the optical density of the atomic cloud and C is the contrast of the measured beat-note signal [54].
The long time regime is reached when $N_P \gg M^{-2}$: in this regime the atomic distribution becomes very narrow ($\Delta J_Z^2 \ll 1$), which is a signature of a collective spin squeezed state.

The advantage of heterodyne detection is that allows to be limited by the shot noise from the weak probe (i.e. one of the sidebands) that contains less photons than the strong carrier used to beat the probe. If N_C is the number of photons in the carrier, N_S the number of photons in the probe and N_e is the photon equivalent noise due to the detection electronics the *signal-to-noise ratio R* is then:

$$R \propto \sqrt{\frac{N_C N_S}{N_C + N_S + N_e}}. \tag{4.17}$$

If the carrier is strong enough ($N_C \gg N_S, N_e$) the signal-to-noise ratio becomes is limited by the number of photons in the sideband N_S i.e. by the shot noise of the weak probe. Further analysis about the noise induced in the measurement are reported in [9].

4.3.2 Feedback using weak measurements

A noise, homogeneous over the size of a trapped ensemble, affects all the atoms in the same way; if there is a sufficient number of atoms in the ensemble it is possible to measure the effect of the collective noise with a weak measurement

that provides neglegible perturbation on the state of the individual systems [39]. This section reports the results of the latest published article [55] by the BIARO group, at the time of the writing of this thesis.

The rubidium 87 atoms that form the ensemble are prepared in a coherent superposition of the two ground hyperfine levels $|0\rangle = |F = 1, m_F = 0\rangle$ and $|1\rangle = |F = 2, m_F = 0\rangle$ of the electronic ground state $5^2S_{1/2}$ and can be manipulated with a microwave field resonant with the 6.835 GHz transition between the two levels. The starting coherent spin state is polarized on the x axis of the Bloch sphere $|\theta = \pi/2\rangle$[4] (see appendix C).

The population difference is weakly measured with a frequency modulated probe in the configuration of Fig: 4.7b: the sidebands are phase-shifted with opposite sign by the two atomic populations due to their opposite detuning with respect to the transitions to $|F'\rangle$ from $|F = 1\rangle$ and $|F = 2\rangle$.

The noise is modeled through random collective rotations implemented using microwave pulses that rotate the Bloch vector around the Y axis [55]. The noise leaves the collective state in a statistical mixture of all the states that can be generated by the noise, decreasing the coherence of the initial state (and decreasing the lenght of the Bloch vector from the starting value of $J = N_{at}/2$). Two models for the noise are described in the paper [55]: a binary random collective noise where the collective Bloch vector is subjected to rotations of fixed angle and random direction ($+\alpha$, $-\alpha$), and an analog collective noise where both the direction and the angle are randomly generated. For the purpose of this work it is sufficient to describe the binary collective noise.

The binary random collective rotation transforms the initial CSS into a balanced statistical mixture of the states $|\pi/2+\alpha\rangle$ and $|\pi/2-\alpha\rangle$, decreasing the coherence of the state from unity to $\eta_\alpha = \cos\alpha$.

After each noise pulse J_z is optically measured and a counter rotation of magnitude α is applied to the ensemble. Since the measurement has to have a small back-action on the ensemble the its uncertainty σ has to be larger than the projec-

[4] This is the state after the first beam splitting in a Ramsey interferometer and corresponds; the average difference of the population between the two considered levels is $\langle J_z\rangle = 0$.

tion noise:

$$\sigma \gg \sqrt{N_{at}}. \tag{4.18}$$

Nevertheless for large CSSs the uncertainty is small compared to the collective spin

$$\sigma < J, \tag{4.19}$$

therefore a weak measurement may provide precise information about the rotation. Knowing the value of α, as in the binary noise model, it is sufficient to detect the correct emisphere in wich the Bloch vector lies; the probability to perform the correct detection is:

$$p_s = \int_0^\infty P(m_0|-\alpha)\mathrm{d}m_0 = \frac{1}{2}\left[1 + erf\left(\frac{\sqrt{2}J\sin\alpha}{\sigma}\right)\right], \tag{4.20}$$

where $P(m_0|-\alpha)$ is the probability to obtain m_0 when measuring J_z given a noise rotation of $-\alpha$.

After the correction the system is in a statistical mixture of three states: $|\pi/2\rangle$ wich is the initial state and is recovered with probability p_s and $|\pi/2 \pm 2\alpha\rangle$ that are states that arise after a wrong correction that doubles the rotation angle.
The coherence of this statistical mixture is

$$\eta_\alpha^{out} = [p_s + (1-p_s)\cos(2\alpha)]e^{-\gamma N_{ph}}. \tag{4.21}$$

The exponential factor takes into account the spontaneous emission induced by the N_{ph} photons in the probe and is adjusted with an experimentally determined coefficent γ that depends on the resonant optical density. The spontaneous emission due to the carrier is small compared to that of the sidebands so N_{ph} refers to the number of photons in the latter.
The ensemble contains about 5×10^5 atoms optically trapped at $10\mu K$ by a laser beam at $1550nm$. The $D2$ transition, used to determine the population difference with a probe at $780nm$, is broadened in a spatially inhomogeneous way due to the Gaussian shape of the trapping beam (see Fig: 4.4b for a qualitative representation of the light shift of the relevant levels that induces the broadening). Compensation of the differential lightshift that produces this effect is discussed in section

4.4 from a theoretical point of view whereas chapter 5 is devoted to the realization of the *servo controller* used to stabilize the power of the laser source for the compensation.

The measurement of the population difference is realized with the configuration depicted in Fig: 4.7b, where each sideband probes the population of one of the two relevant levels with the same magnitude and opposite sign for the couplings. The probe induced light shift is canceled compensating the effect of the carrier with the one of the sidebands.
The measurement of J_z uses a $1.25\mu s$ long pulse; the detected signal is demodulated to get the population difference an analogicaly integrated to get the mean value over the pulse lenght. The integrated signal is digitalized and sent to a microcontroller unit (MCU) that treats it in real time to get the sign of J_z. The MCU controls the rotation direction for the α correction pulse that closes the feedback loop.

To determine the coherence of the atomic state, after the correction pulse a $\pi/2$ rotation is induced on the ensemble to complete a Ramsey type measurement. Results after one feedback loop are presented in Fig: 4.8. To study how the feedback scheme can protect a CSS over time in the presence of noise, an iteration of the random collective noise, population measurement, correction sequence is realized 200 time on the same atomic sample. Here the number of photons in each sideband has been adjusted to 1.4×10^7.
The results are representend in comparison to the open loop situation (no correction applied) under two different forms: the first is a measure of the state occupancy, which is the probability to be in a given state, versus time averaging the results of 200 experimental runs. In the closed loop case, the system spreads from $|\pi/2\rangle$ to the two poles ($|0\rangle$, $|\pi\rangle$), and at a slower rate to $|3\pi/2\rangle$. In open loop after a few iterations the state vector reaches a balanced statistical mixture of four states: $\{|0\rangle, |\pi/2\rangle, |\pi\rangle, |3\pi/2\rangle\}$ for an even number of iterations, and $\{|\pi/4\rangle, |3\pi/4\rangle, |5\pi/4\rangle, |7\pi/4\rangle\}$ for an odd number. Results are presented in Fig: 4.9(a)-(b).
The second representation of the results of this experiment is the coherence of the

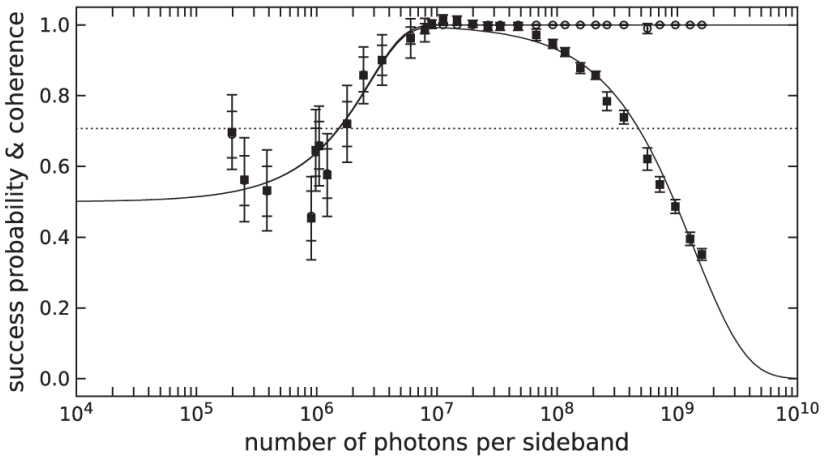

Figure 4.8: Coherence of the collective spin state after one noise-correction cycle as a function of the number of photons per sideband (solid squares). Success probability of the probe pulse (open circles). Solid line is a fit of the remaining coherence data with Eq. 4.21; dashed line is a fit of the probability of success data with Eq. 4.20; dotted line indicates the coherence after the random collective noise. Image taken from [55]

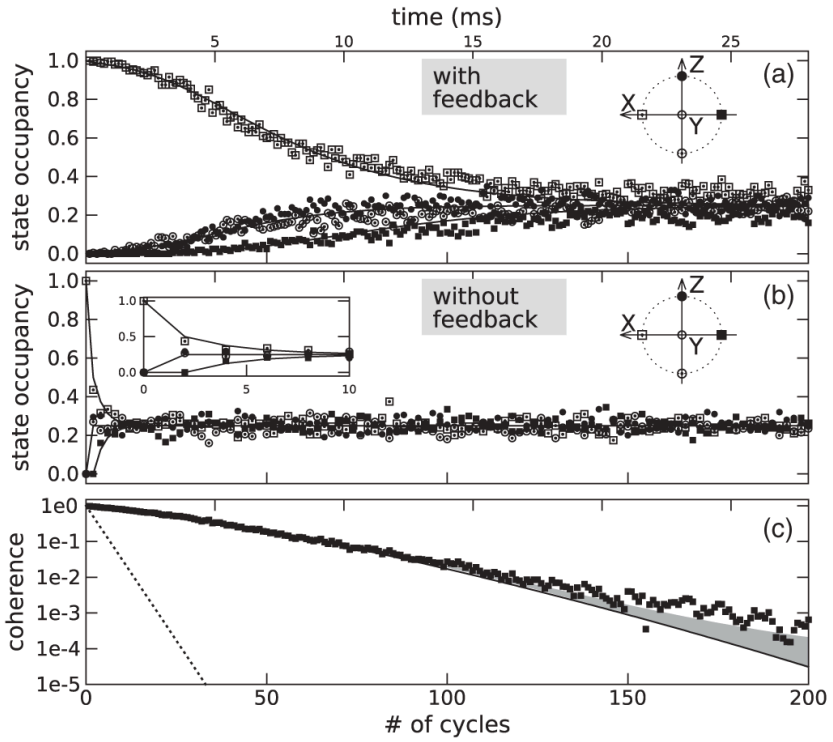

Figure 4.9: Image taken from [55]

state protected through feedback versus the coherence of the open loop situation presented in Fig: 4.9(c). In open loop after $N = 10$ cycles the remaining coherence is 0.03 whereas with feedback it reaches 0.77.

We end this section with the words of the authors of the paper [55]:

> To summarize, we have demonstrated the partial protection of an atomic CSS from the decoherence induced by RCRs around a fixed axis, using feedback control based on weak nondestructive measurements. The method can be generalized to rotations around an arbitrary axis of the Bloch sphere: one could consecutively read out J_x, J_y and J_z and correct with suitable rotations. Compared to spin-echo

techniques, relying on temporal invariance of the noise, our feedback method allows the compensation of time dependent noise, provided that the time evolution is slower than the correction time. By increasing the effective on-resonance optical depth, the feedback scheme could be implemented in the projective limit to deterministically prepare nonclassical states, using measurement based spin squeezing.

4.4 Compensation of the differential lightshift

The trapping radiation (at 1560*nm* in the BEC realization and at 1550*nm* in the feedback experiment) induces a differential light shift on the D2 transition used for the non destructive probing of the population difference. This differential light shift is of central importance for the in-situ characterization of the dipolar potential (see section 4.1.1, refer to [10], [53]) but is a limiting factor if we want to manipulate or probe the trapped atoms with a beam (quasi)resonant with the atomic transition $5S_{1/2} \rightarrow 5P_{3/2}$ as in the case of the QND measurement for the feedback scheme discussed in Section 4.3.2.

In the following section we discuss (using [53] as a reference) the compensation of this trapping beam-induced light shift using a 1529*nm* laser spatially overlapped to the trapping radiation.
Radiation at 1529*nm* and 1550*nm* is mainly coupled to three transitions:

$$5P_{3/2} \rightarrow 4D_{3/2}; \quad \lambda = 1529.261nm; \quad d = 3.633ea_0; \tag{4.22a}$$

$$5P_{3/2} \rightarrow 4D_{5/2}; \quad \lambda = 1529.366nm; \quad d = 10.899ea_0; \tag{4.22b}$$

$$5P_{3/2} \rightarrow 6S_{1/2}; \quad \lambda = 1366.875nm; \quad d = 6.047ea_0; \tag{4.22c}$$

where λ is the wavelength associated with the transition and d is the dipole matrix element expressed in units of the fundamental charge e and the Bohr radius a_0.
It is therefore possible to calculate the scalar polarizability (see Chapter 3) induced by the radiation of frequency ω as:

$$\alpha_v = \frac{2}{3\hbar}\frac{1}{2J_v+1}\sum_k \frac{\omega_{kv}}{\omega_{kv}^2-\omega^2}d_{kv}, \tag{4.23}$$

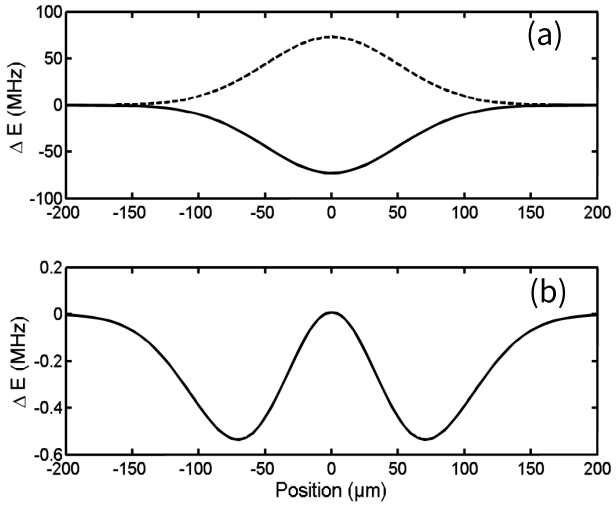

Figure 4.10: a) Light shift of the $5P_{3/2}$ level induced by the trapping radiation at 1550*nm* (solid line) and by the 1528.7*nm* beam (dotted line). b) Residual light shift after compensation. Image taken from [53]

where J_v is the total angular momentum of the state $|v\rangle$, ω_{kv} is the transition frequency between the levels $|k\rangle$ and $|v\rangle$ and d_{kv} represents the dipole matrix element between the two levels. The resulting scalar polarizabilities are:

$$\alpha^{1550}_{5P_{3/2}} = 4.736 \times 10^{-37} Jm^2/W; \tag{4.24a}$$

$$\alpha^{1528.7}_{5P_{3/2}} = -1.422 \times 10^{-35} Jm^2/W. \tag{4.24b}$$

As expected the signs of the polarizabilities are opposite, it is then possible to compensate the differential light shift from the trapping laser overlapping it with the 1528.7*nm* with the correct optical power ratio between the two. Equations 4.24 suggest that the optical power of the compensating beam should be approximatively 500 times less than the optical power of the trapping laser.

The light shift induced by the 1550*nm* laser on the $5P_{3/2}$ level for an intracavity optical power of $10W$ reaches $170MHz$ at the crossing of the beams ($\approx 85MHz$ for each arm of the trap. See Fig: 4.10a). This value is close to the detuning used to probe the J_z operator with QND measurements: it is not possible to

probe the population without a proper compensation.
Fig: 4.10b shows the calculated residual light shift after compensation with the $1528.7nm$ beam; residual light shift is due to the unperfect overlapping of the beams in the fundamental mode of the cavity.
A first coarse adjustment of the optical power of the laser beam for the compensation is reported in [53] and was used to set the wavelength to $\lambda = 1528.7nm$.
To adjust the optical power in a fine way QND measurements are exploited: intracavity power of the $1550nm$ laser have been set to $10W$ and measurement of J_z have been performed on an ensemble of atoms prepared in the coherent state $|\pi/2\rangle$. When no trapping radiation is present the measurement yields $J_z = 0$, as expected. If the atoms are probed when they are trapped, due to the differential light shift, the result of the QND measurement is different from zero. To obtain the compensation the optical power of the $1528.7nm$ radiation has been adjusted to the value that allows a QND measurement of J_z equal to zero.

In [53] the results of this adjustment are reported (see Fig: 4.11): the light shift is adjusted for an optical power of 39.6 ± 2.5 mW. The relative uncertainty is of 13%, a value that yields an uncertainty of about $10MHz$ on the residual light shift, a value much higher than the expected residual light shift $1.3MHz$.

For a correct compensation of the differential light shift a *power servo controller* for the compensation beam have been realized as described in Chapter 5.
The residual light shift after compensation is about[5] $0.7MHz$ which is small compared to the transition linewidth $\Gamma = 2\pi \times 6MHz$.

[5] See Supplemental Material of [55] at http://link.aps.org/supplemental/10.1103/PhysRevLett.110.210503

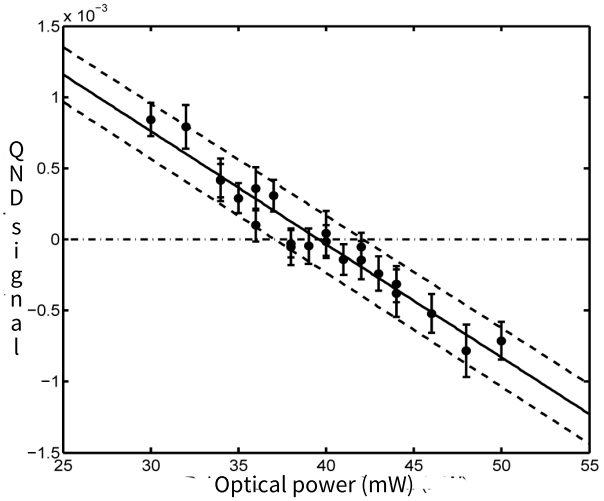

Figure 4.11: QND measurement (a.u.) of J_z for trapped atoms as a function of the optical power of the 1529*nm* compensation laser beam. Image taken from [53]

Chapter 5

SERVO CONTROLLER OF THE POWER OF A FIBER LASER

THe compensation of the differential light shift induced by the trapping laser requires the injection of a laser beam at 1529*nm* in the fundamental mode of the cavity. The optical power of the 1529*nm* has to be stable beam because amplitude noise induces heating in far-off resonant optical dipole traps through the parametric heating mechanism [50]. On the other hand the optical power has to be adjustable to find the right value for an optimal compensation as described in Section 4.4.

This chapter is devoted to the conception and realization of a *power servo controller* for the compensation beam through the use of a negative feedback system. In section 5.1 is treated the realization of an appropriate front end for the photodiode used in the servo controller. Section 5.2 reports the description and characterization of the actuator used in the feedback loop which is a *Variable Optical Attenuator* (VOA). In the last part of the chapter, section 5.3, the electronic board that implements the feedback loop for the power servo controller is treated.

5.1 Transimpedence for the photodiode

The first block of the power servo controller is the photodiode[1] with its front end. A photodiode produces a photocurrent I_d when hit by light; the current is proportional to the number of photons in the beam (i.e. to the power of the beam). The photocurrent is transformed in to a voltage $V(t)$ by the front end, in our case a *transipendence*. There are two factors to consider when designing a front end: the cutoff frequency f_c and the Signal to Noise Ratio (SNR).
The cutoff frequency corresponds to the $-3dB$ corner in the characteristic of the transimpedence. The higher it is, the faster the transimpedence.
The SNR is defined as:

$$SNR = \frac{i_d^2}{\sum_N i_N^2}, \tag{5.1}$$

where the sum is over all the noise currents i_N. We want to be limited by the shot noise of the photocurrent $i_{sn} = \sqrt{2ei_d}$.

The simplest front end is a simple resistor R_L. The photocurrents across the resistor is transformed into a voltage. The photodiode has a terminal capacitance $C_d = 12pF$. The cutoff frequency is therefore [30]:

$$f_c = \frac{1}{2\pi R_L C_d}. \tag{5.2}$$

A low value for R_L is necessary to have high bandwidth, but an high value is required to have an high SNR since the Johnson noise of the load resistor is: $i_{NR} = \sqrt{\frac{4kT}{R_L}}$.
To be limited by the shot noise of the photocurrent we can safely lower the value of R_L to the point where $i_{NR} = i_{SN}$:

$$i_d R_L = 2kT/e, \tag{5.3}$$

where the right side of the equation is equal to $51mV$ at $300K$.
The loss in the SNR is about $1dB$ for $i_d R_L \geq 200mV$; this limits the value of the load resistance to $R_L \geq 200mV/i_d$.

[1] We used a photodiode from Hamamatsu, model G8376

5.1.1 Transimpedence design

A transimpedence amplifier is a more sofisticated front end that makes use of an operator amplifier (OpAmp) and of a feedback realized with a capacitance C_f and a resistor R_f (see Fig: 5.1). The photodiode is connected to the inverting

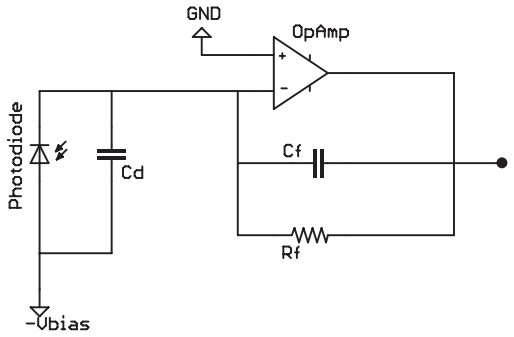

Figure 5.1: Scheme of a typical transimpendence amplifier: C_f and R_f are the feedback capacitance and resistance.

input of the OpAmp while the non-inverting input in connected to ground: if the operator amplifier is ideal and operates in the linear regime the photodiode is connected to a virtual ground. The inverting input of the OpAmp draws no current but the feedback forces the voltage there to be close to zero at all the times [30].
The cutoff frequency of the transimpedence is

$$f_c \approx \frac{\sqrt{f_{RC} f_A}}{2}, \tag{5.4}$$

where $f_{RC} \frac{1}{2\pi R_f \sum C}$ is the frequency cut of a low pass filter[2] and f_A is the bandwidth of the OpAmp.
The SNR equals that of the same amplifier used as a unity-gain buffer on a photodiode plus load resistor [30] and, provided that the voltage noise of the amplifier e_{Namp} is very low, the noise rising from the amplifier is negligible. The transimpedence therefore provides a higher cutoff frequency at a little price in terms of SNR.

[2]The sum is over all the capacitances in the transimpedence: C_d, C_f and the capacitance of the OpAmp.

We opted for an OpAmp[3] with bandwidth $f_A = 325MHz$ and adjusted the values of the feedback resistance and capacitance to $R_f = 39K\Omega$ and $C_f = 1pF$. The attained cutoff frequency is $f_c \approx 7Mhz$.
This value is more than enough to detect the amplitude noise that we want to remove in the dipole trap: parametric heating is induced by amplitude variations with frequency comparable with the second harmonic of the trap frequency [50]. A discussion of the trap frequencies is reported in Section 4.1.3: the order of magnitude is $1kHz$.

5.2 Actuator

The second component for the power servo controller is an actuator. We chose as actuator a variable optical attenuator (VOA), a device used to reduce in a controlled manner the optical power of a signal in a fiber cable.
A typical VOA uses a variable neutral density filter to provide attenuation. Through an input modulation (either mechanical or electonic) the density filter is moved and the user can vary the optical output power.
VOAs are usually wavelength insensitive, mode insensitive and stable. The main disadvantage is that they usually are higly nonlinear[4] and require calibration.

5.2.1 A mechanism to build a Variable Optical Attenuator.

There exist different patents for different mechanisms for a VOA. In this section we will explain the content of patent [49] made by Robinson in 2000, just to make a simple example of the principle used to provide optical attenuation. The device works as follows: a waveguide (for instance a fiber cable) drives the light to a lens with focus on a moving mirror. If the mirror is in his standard position (see fig:5.2) the light back reflected to the lens and enters in an output optical waveguide *undisturbed*. Moving the mirror provides a way to decrease the amount of light in the output.

[3] Texas Instruments THS4631

[4] As we will see for the one we used, as reported in section 5.2.2

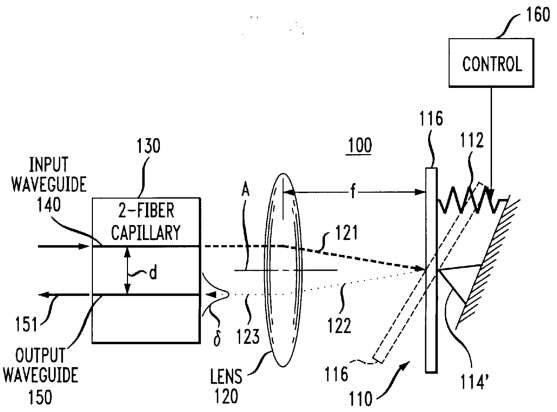

Figure 5.2: Scheme of the optical attenuator described in [49]; the solid line shows a position with no attenuation, dashed line is a possible attenuation position. Image taken from the patent.

The mirror is moved using a semiconductor micro-electronical optical device that allows different levels of optical attenuation.

5.2.2 Characterization of the VOA

In this section we report the charcterization of the variable optical attenuator[5] used to build the amplitude lock.
The VOA provides electrical control of the optical power. It is driven by $0-4.2V$ input bias and with nominal attenuation of $1dB$ at $0V$ and $34dB$ at $4.2V$. The working wavelenghts range is $400-1800nm$. The nominal bandwidth is $5KHz$: the device is protected by an integrated microcontroller from higer frequencies.

The test has been made using a $1550nm$ *distributed feedback* (DFB) fiber laser diode[6] mounted on a *butterfly laser diode mount*[7] with Thorlabs drivers for current and temperature control. The output power of the laser is controlled by a bias current. Working temperature for the laser diode is 26°C. The output fiber cable

[5] AGILTRON 1550NnaoSpeed PM HP VOA
[6] Fitel FRL15DCWD-A81-1550-C DFB laser module
[7] Thorlab LM14S2 Butterfly Laser Diode Mount

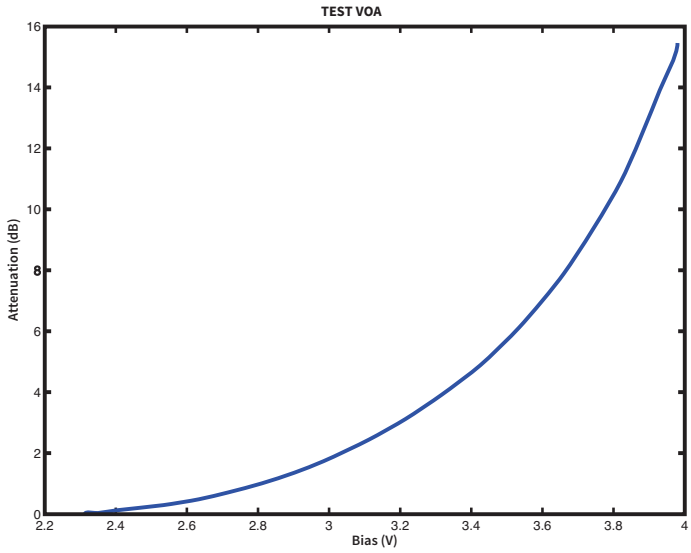

Figure 5.3: Test of the attenuator. Control voltage range is 0-4V.

from the DFB is connected directly to the VOA. The input bias for the attenuator is provided by a custom circuit board that allows the control of the bias from $0V$ to $4V$. The circuit must avoid the output voltage to overcome the $4V$ limit, so to protect the VOA: we decided to mount a $4V$ Zener diode between the output and the ground

We measured the output power with an optical power meter. We normalized the output power to the maximum value and proceeded in converting the attenuation in dB:

$$dB(W) = 10log_{10}(\frac{P}{P_{max}}) \tag{5.5}$$

The results of this test are shown in Fig: 5.3. Since the obtained attenuation is lower than the nominal maximal value we proceeded with a new test.

For the new test we used a wave generator[8] and measured the bias voltage (V_{bias}) with an oscilloscope[9]. The input range varied from $0V$ to $4.16V$, whereas the bias current of the DFB was set to $180mA$.

[8] AGILENT 33250A

[9] TEKTRONIX TDS 1002

The results are shown in Fig: 5.4 and Fig: 5.5. As declared by the producer we have a maximum attenuation of $34dB$ (at $4.16V$). The behaviour of the VOA is highly nonlinear.

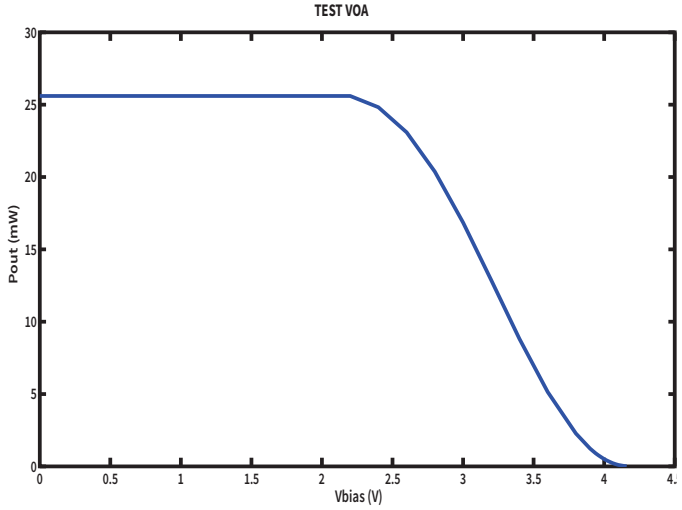

Figure 5.4: Test of the attenuator, where the optical power (mW) after the VOA is measured as a function of the input voltage

We tested the minimun attenuation provided by the VOA (i.e. the attenuation when we provide vanishing bias voltage, compared to the optical power of the laser measured directly after the DFB). The test was made with a current bias of $64.5mA$ and gives as a result an attenuation of $1.04dB$, compatible with the $1dB$ declared by the producer.

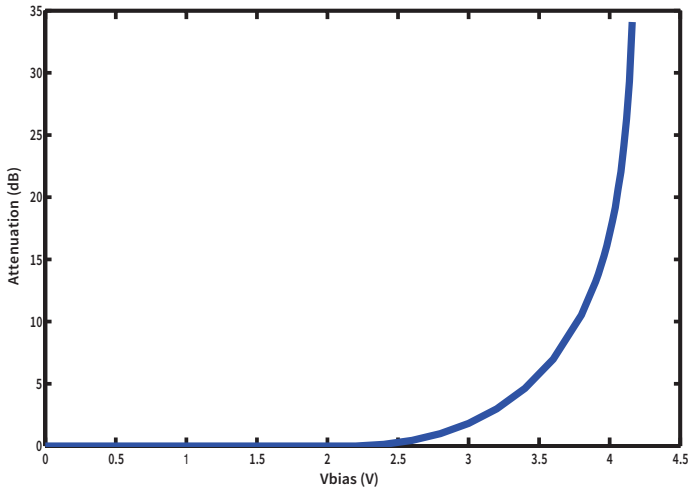

Figure 5.5: Test of the attenuator: the attenuation (dB) of the VOA is plotted as a function of the input voltage

5.3 Electronic board

The purpose of this section is to explain how we built the electronic board to produce the error signal to implement the feedback mechanism. We drive the laser diode with some current and at a given temperature and get an optical power as output that is transformed in a voltage through the photodiode-transimpedence described in Section 5.1. The signal from the transimpedence is compared to a reference value, suitably filtered, amplified and used to drive an actuator on the controlled quantity. The feedback scheme is shown in figure D.1.
The electronic board we implemented allows the selection of the reference value, performs the comparison with the signal from the photodiode and produces as output the control voltage for the VOA.

5.3.1 Proportional-Integral-Derivative controller

A Proportional Integral Derivative (PID) controller is a widely used servo mechanism adopted in feedback (control) loops. It calculates the error between the set value and the input and attempts to minimize it.
In this section we describe the three components of a PID controller: a proportional amplifier that produces a signal proportional to the present error, an integrator amplifier that takes into account the accumulation of past errors and a differential amplifier that tries to anticipate the future errors.

Proportional amplifiers

This is the most simple instrument and has the function to amplify the difference between the set value and the input from the photodiode. The two signals are subtracted using an Operational Amplifier in the configuration of Fig: 5.6. The ratio of the feedback resistor R_f and the input resistors R_{in} sets the proportional gain:

$$V_{out} = -V_{in}\frac{R_f}{R_in}, \tag{5.6}$$

where V_{in} is the difference between the set value and the signal from the transipendence and V_{out} is the error signal produced by the proportional amplifier.

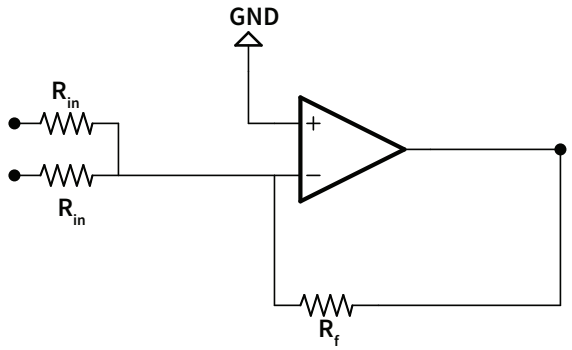

Figure 5.6: Proportional amplifier.

The proportional gain has to be tuned: if the value is too high the system may become unstable whereas if it is too low the controller becomes less sensitive to disturbances.

Integrator amplifiers An integrator amplifier is realized with a capacitance C in the feedback path of an operational amplifier as in Fig: 5.7. If the OpAmp works

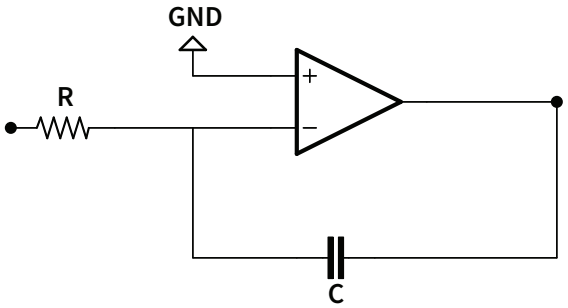

Figure 5.7: Scheme of an integrator amplifier. The gain is decreasing linearly at -3dB/decade.

in the linear regime the inverting input is a virtual ground. For an input voltage $V_{in}(t)$ the current across R is then $i(t) = V_{in}(t)/R$. The behaviour at the capacitance

is $i(t) = C\frac{\mathrm{d}V(t)}{\mathrm{d}t}$. Therefore we have:

$$\frac{V_{in}(t)}{R} = C\frac{\mathrm{d}V(t)}{\mathrm{d}t}, \tag{5.7}$$

that has as a solution for:

$$V = -\frac{1}{RC}\int_0^T V_{in}(t)\mathrm{d}t. \tag{5.8}$$

The output signal is the integral over time of the input voltage. The amplifier gain decreases linearly as a function of the frequence at a constant ratio of $3dB/decade$. The frequency for unity gain[10] depends on the feedback capacitance and on the input resistance: $f_{0dB} = \frac{1}{2\pi RC}$. At low frequency the gain increases due to the capacitor behaviour: in the limiting case of DC the capacitor acts as an open circuit and the gain becomes infinite for an ideal OpAmp.
It is possible to add a feedback resistor $R_f$in parallel with the feedback capacitance to limit the gain at low frequency. The feedback becomes therefore a high pass filter with cutoff frequency $f_c = R_f/R$.
In such a situation the transfer function is

$$\frac{V_{in}}{V_{out}} = -\frac{R_f}{R}\frac{1}{1+i\omega CR_f}, \tag{5.9}$$

where ω is the frequency of V_{in}.
An integrator amplifier produces a steadily changing output for a constant input voltage: if the input comes from a proportional amplifier, the signal produced by the integrator amplifier is proportional to the error over time.

Differential amplifiers A differential amplifier is realized with a resistance R at the feedback side of an OpAmp and a capacitance C at the input side (see Fig: 5.8). The inverting input is a virtual ground so V_{out}, the voltage across the resistor, is related to V_{in}, the input voltage, by:

$$V_{out} = -RC\frac{\mathrm{d}V_{in}(t)}{\mathrm{d}t}. \tag{5.10}$$

[10]Or crossover frequency, where the gain is $0dB$.

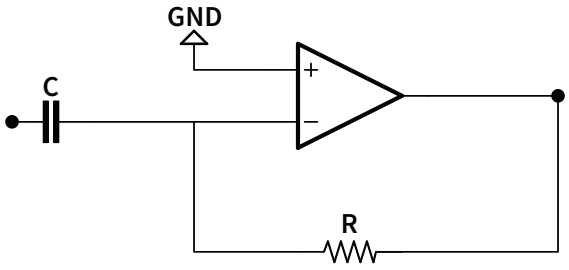

Figure 5.8: Scheme of an differential amplifier.

The output signal is proportional to the rate of change at the input with opposite sign: a steadily increasing input voltage will produce a constant negative output voltage, *vice versa* a steadily decreasing input will produce a constant positive output.
At low frequencies the capacitor acts as an open circuit and a vanishing current flows through it and through the resistor: the output voltage is small whereas at high frequencies the system becomes unstable. Since the correction is based on the present rate of change, a differential controller is used to foreview the changing in the error signal to anticipate corrections. The use of a differential controller is to foreview the changing in the error signal and to provide correcction.

In our design we decided not to use a differential controller because we need to switch between two different reference values and a differential controller could be too sensitive to such a sudden change.

5.3.2 The electronic circuit for the servo controller

The electronic board for the servo controller of the power of the 1529*nm* fiber laser is made of the following parts (see FigureD.2):

1. transimpedence for the photodiode;
2. proportional amplifier;
3. integrator amplifier;

4. analog switch between two adjustable set values;

5. adjustable overall gain;

6. a switch to turn on/off the feedback.

The power of the $1529nm$ fiber laser is measured with a photodiode from Thorlabs[11]. The board is connected to a $\pm 15V$ supply.

Transimpedance The photocurrent is sent to the transimpedence that has been realized with a feedback resistance $R_f = 100k\Omega$. The value of the feedback resistance has been increased, compared to the one used to test the VOA (see Section 5.1.1), to improve the SNR.

Proportional amplifier The proportional amplifier has been realized with a gain $G = 6$ using an input resistors value $R_{in} = 20k\Omega$ and as feedback resistor $R = 120k\Omega$.

Integrator amplifier The output voltage from the proportional amplifier serves as input value for an integrator amplifier with the low frequency cut set to $f_c = 4.7Hz$.

Set values The set values range from 0 to $10V$. A stable $10V$ reference has been used to provide the voltage across two potentiometers that allow to adjust the set values. The analog switch is driven by a TTL signal. The VOA used as actuator has a bandwidth of $5kHz$: to prevent the integrated microcontroller to stop the VOA we added a low pass filter with cut at $720Hz$ between the analog switch and the proportional amplifier. Two different set values for the optical power are required to compensate the differential light shift while performing:

- weak measurements on the ensemble;
- the loading of the dipole trap from the MOT.

[11] Thorlabs PDA10CF.

Overall gain and inverter The overall gain may be adjusted using a $20k\Omega$ potentiometer at the inverting input of an OpAmp with feedback resistance $R = 100k\Omega$. This last OpAmp serves as an inverter to have a positive voltage at the output to drive the actuator.

On/Off switch A manual switch has been added before the output SMA connector that goes to the VOA. This switch allow to turn on the feedback loop, setting as output the voltage value from the inverter, and to turn to an *open loop* configuration, connecting the output to ground. A $5.1V$ zener diode has been added at the output so as to protect the VOA.

The custom electronic board has been designed using EAGLE cad[12] and then realized on a printed circuit board (PCB). The electronic components has been soldered in the electronic laboratory at the Laboratoire Charles Fabry - Institut d'Optique Graduate School.

5.3.3 Test of the electronic board

The test of the electronic board has been done using the $1550nm$ laser used to test the VOA (see Section 5.2.2).
The TTL signal for the switch between the two set values was provided by plugging/unplugging a *lemo* connected to a $4.5V$ battery.
The transimpedence during the test was set to have a maximum of $15.4V$ when the optical power was $25.60mW$[13] . The low set value, used to lock the amplitude of the beam to perform weak measurements, was adjusted to $50mV$. The high set value, needed to stabilize the optical power for the loading of the dipole trap from the beam[14], was set to $9.6V$. The output of the transimpedence was monitored on

[12] www.cadsoftusa.com

[13] The laser was driven with 180mA.

[14] To efficiently load the dipole trap from the MOT the trap depth should be as high as possible. A high power from the trapping laser beam is required, therefore high optical power from the compensation beam is required as well.

an oscilloscope.

When the feedback loop was connected the system started to oscillate around the desired set value. After checking all the electrical connections we isolated and checked each component of the electronic board. Since we didn't find the source of oscillations in the electronics we concluded that it could have been in the VOA. We added a low pass (cut frequency $f_c \approx 15Hz$) filter right before the output of the electronic board; this allowed the the feedback system to work. Further analisys on the source of oscillations have not been possible due to time constraints.

We measured the time response of the system when switching between the two set values. The response is limited by the low pass filter used to prevent the microprocessor from stopping the VOA. Therefore the change between the value of optical power of the laser, used for the compensation of the differential light shift for the loading of the dipole trap on one side and for the weak measurement on the other, is rather slow ($700Hz$ the response frequency).

Setting the laser level to $10V$ we could easily achieve a switch between the first set value at $9.6V$ and the second at $50mV$ with a maximum noise of $5mV$ on the low level. This means two and a half order of magnitude between a possible high and a possible low level with a maximum error of 10% on the low level and a negligible error on the high level.

The stability of the system has been verified adding a modulation of $50mV$ with a sinosiduidal signal when the driving current is around $160mV$ and verifying that there is no variation on the output level when the feedback system is on.

CONCLUSIONS

In this thesis we reported the realization of a servo controller of the power of a fiber laser. This device is used to adjust and stabilize the optical power of a fiber laser in a high finesse resonator. The stabilized beam is used to compensate the differential light shift induced on Rubidium atoms by a trapping radiation. The compensation of the differential light shift plays a critical role in the loading of atoms in the dipole trap and in the realization of precise QND measurements of the populations on different hyperfine levels of the atomic groud state.

QND measurements are now used as a part of a feedback scheme that protects a coherent spin state from the naturally occurring decoherence: if such a scheme succeds to be generalized it will be useful in the domain of interferometry and quantum information.

One goal of the BIARO experiment is the realization of collective spin squeezed states: a theoretical model for the realization has been produced by the memebers of the group but, at the moment of the writing of this thesis, the experimental realization has failed to produce such states. The realization of SSS should allow to overcome the standard quantum limit and may bring improvements in the domain of metrology. Interferometers and phase dependent detectors may improve in sensibility.

Weak measurements, only introduced in this work, may be used to answer open questions about the nature quantum processes and may be exploited to obtain information that were thought meaningless only twenty years ago. The field of quantum measurements takes benefit from the continuos improvement of experimental techniques. We are now at a point where theorists and experimentalists

may work side by side and not one ahead of the other. We expect important results in the forecoming years from the experimental front that may stimulate a better or more complete theory of quantum measurement. At the same time we expect theorists to give rise to new questions or paradoxes arising from the quantum world that would set new goals for experimentalists.

Appendix A

RUBIDIUM 87 D2 STRUCTURE

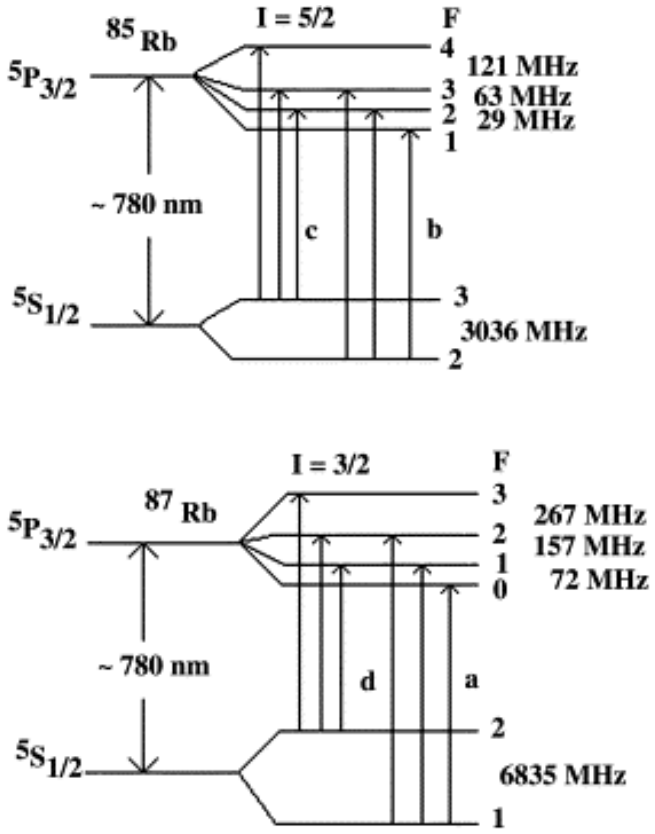

Figure A.1: Rubidium 85 and 87 D2 atomic line. Image taken from [11]

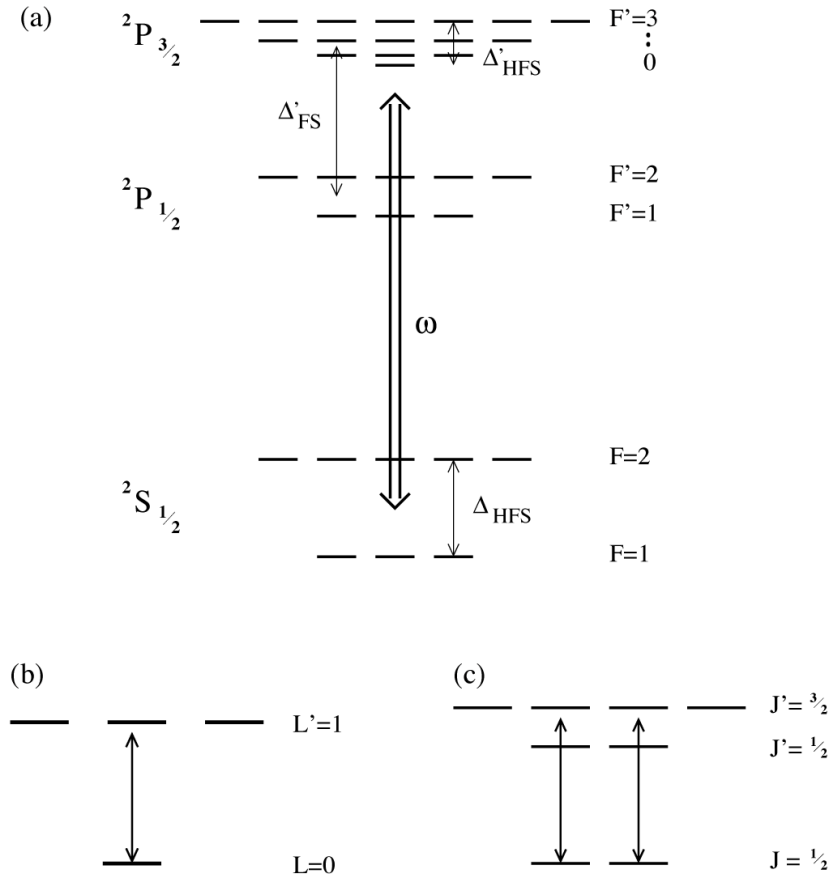

Figure A.2: Scheme for an $ns \rightarrow np$ transition of an alkali. a) Full scheme including fine (Δ_{FS}) and hyperfine (Δ_{HFS}) splitting. b) Negligible fine and hyperfine splitting. c) $\Delta_{HFS} \ll \Delta_{FS}$, only the fine structure is displayed. Image taken from [27]

	λ_{D_2,D_1} (nm)	$\Delta'_{\mathrm{FS}}/2\pi$ (GHz)	I	$\Delta_{\mathrm{HFS}}/2\pi$ (MHz)	$\Delta'_{\mathrm{HFS}}/2\pi$ (MHz)	$\Gamma/2\pi$ (MHz)	T_{rec} (μK)	h_{rec} (μm)
^{6}Li	670.9, 670.9	10	1	228	4.6	5.9	7.1	1000
^{7}Li			3/2	804	18		6.1	740
^{23}Na	589.0, 589.6	510	3/2	1772	112	9.9	2.4	88
^{39}K	766.7, 769.9	1500	3/2	462	34	6.2	0.84	18
^{40}K			3	1286	100		0.81	17
^{41}K			3/2	254	17		0.79	16
^{85}Rb	780.0, 794.8	7200	5/2	3036	213	5.9	0.37	3.7
^{87}Rb			3/2	6835	496		0.36	3.5
^{133}Cs	852.1, 894.3	16600	7/2	9192	604	5.3	0.20	1.3

Figure A.3: Relevant properties of the alkali atoms for optical dipole trapping. Table taken from [27]

Appendix B

CLASSICAL MODEL FOR LASER RADIATION PRESSURE

THis Appendix is meant to introduce optical trapping in a semiclassical fashion. An hystorical track of the use of laser to trap neutral particles can be found in the 2006 book from A. Ashkin [7].

Order of magnitudes involved

Consider a monochromatic laser beam of wavelenght ν and power P. We know that the energy of each photon is $E_{ph} = h\nu$ and, even though photons are massless at rest, we can associate an effective mass due to the Einstein relation to find that each photon carries a momentum $m_{eff}c = h\nu/c$.
The rate of photons per second in the beam is simply $P/E_{ph} = P/h\nu$ thus a fully reflecting object hit by the beam experiences a momentum kick (per second) of the order of $2h\nu/c$ times $P/h\nu$. Since the momentum variation over time is the force we can simply write:

$$F_{rad} = 2P/c. \tag{B.1}$$

If the laser beam is focused on a particle with linear dimension of the order of λ and reflectivity ρ we get the force $F_{rad} = \rho 2P/c$ acting on a particle with volume $V \approx \lambda^3$.

This means that if $\lambda \approx 10^{-6}m$, $P \approx 1W$ and $\rho \approx 0.1$ then a particle with density $d \approx 10^3 Kg/cm^3$ should accelerate at about $10^5 g$ where g is the acceleration due to gravity.

Transparent spheres in a fluid medium

Suppose we have sferical particles, with diameter d (large compared to the wavelenght λ), in a fluid medium[1]; we can then estimate the effect of a laser beam passing trough the solution. Consider the particle to be in a spatially homogenous field (see figure B.1); to understand the effect of a couple of symmetric rays, belonging to the same wavefront, hitting the particle let's see which path any of the two would follow. The ray a (b) will be refracted following Snell's law both entering and leaving the particle. The ray will leave the particle locally with the same angle it had when it entered but with a global shift in direction due to the curvature of the particle. The change in direction of each ray results in a change of momentum of the ray and therefore the particle is exerting a force on it. The particle experiences an opposite force F_a (F_b) following the third principle of dynamics. The overall effect of the two symmetric rays is therefore a net force on the particle that we call *radiation pressure*.

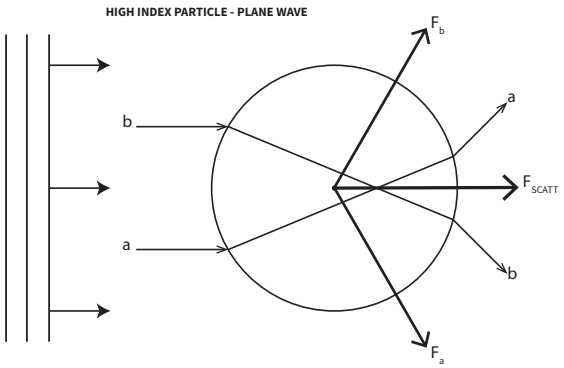

Figure B.1: Simplified ray optics diagram for a high index particle in an homogeneous laser field.

[1] we can imagine a diuted solution of latex spheres in water as in [7]

Consider now a particle in a beam with gaussian profile (see figure B.2): if the particle is not in the exact center of the beam, the net forces of the two rays we are considering will not be equal in magnitude and will therefore give rise to a *transverse force* F_{grad}, dependent on the rate of the refractivity index of the particle to the one of the medium, that will push (or pull) the particle out of (inside of) the beam.

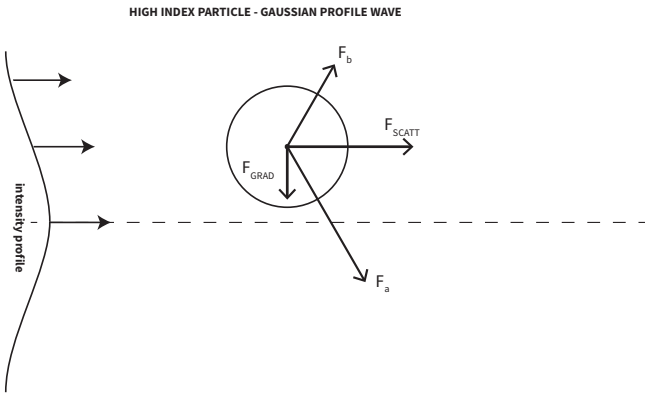

Figure B.2: High index particle in an gaussian laser field. Due to the unbalanced intensity profile there are more rays on one side of the particle. The net effect is that F_a is greater than F_b giving rise to a transverse component of the force F_{grad}.

This is the effect of laser radiation pressure on *macroscopic* particles. It is very insightful to see an effect that can be used to confine particles in a completly classical treatment as the one illustrated throught this section. It is worth noting that two transverse beams would serve as a 3D trap for transparent particles (as observed in [7]).

Appendix C

COLLECTIVE SPIN STATES AND BLOCH SPHERE

We have seen in chapter 2 that when we treat the laser-atom coupling, if we consider the atom as a two-level system, different phenomena occurs, including Rabi oscillations (section 2.1) and light shift of the atomic levels (section 2.2). In this section we want to generalize those results to a system made of many identical particles each of which we will treat as a two-level system; we will refer to them as *collective spin states*.
Before introducing collective spin states it may be useful to briefly resume the *Bloch sphere* representation of a two-level system.

C.1 Bloch sphere

The state of a psudo-spin system is described by a vector in a Hilbert space $\mathscr{H}_2 \equiv \mathbb{C}^2$ where a basis is formed by $\{|a\rangle, |b\rangle\}$. A vector $|\psi\rangle \in \mathscr{H}_2$ is defined by two complex numbers α, β that satisfy $|\alpha|^2 + |\beta|^2 = 1$:

$$|\psi\rangle = \alpha|a\rangle + \beta|b\rangle. \tag{C.1}$$

It is straightforward to write eq. (C.1) as

$$|\psi\rangle = \cos(\theta/2)|a\rangle + e^{i\phi}\sin(\theta/2)|b\rangle, \tag{C.2}$$

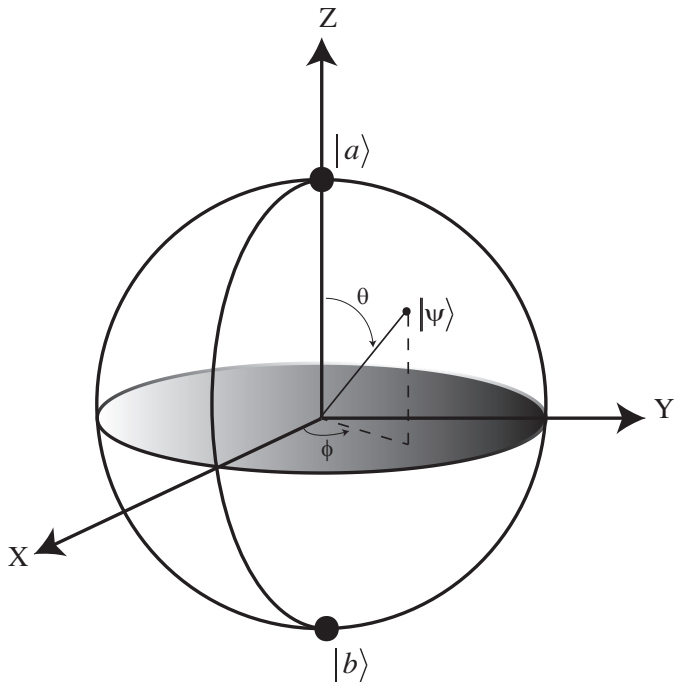

Figure C.1: Bloch sphere.

with $0 < \theta < \pi$ and $0 < \phi < 2\pi$ real numbers. The interpretation of θ and ϕ as spherical coordinates leads to the interpretation of $|\psi\rangle$ as a point on the Bloch sphere. The states that define the basis of the Hilbert space correspond to the north and south pole on the sphere.

The probability to obtain the result $|a\rangle$ when performing a projective measurement is easily computed as $P_a = \cos^2(\theta/2)$ as one would expect.

The evolution of $|\psi\rangle$ on the sphere, due to Schroedinger equation, is a rotation on the surface. We do not enter into mathematical details[1] but simply remind that rotations on a 3D sphere are elements of $SU(2)$. We may define the following

[1] That can be found in any quantum mechanics textbook; see for instance [20]

operators:

$$j_x = \frac{1}{2}\left(|a\rangle\langle b| + |b\rangle\langle a|\right) \tag{C.3}$$

$$j_y = \frac{1}{2}\left(|a\rangle\langle b| - |b\rangle\langle a|\right) \tag{C.4}$$

$$j_z = \frac{1}{2}\left(|b\rangle\langle b| - |a\rangle\langle a|\right) \tag{C.5}$$

that are the generators of the group. The more familiar *Pauli matrices* $\sigma_k = 2j_k$ ($k = x, y, z$) are the expression of the operators in the $|a\rangle, |b\rangle$ basis. For sake of simplicity we remind just the commutation relation between the Pauli matrices

$$[\sigma_i, \sigma_j] = 2i\varepsilon_{ijk}\sigma_k, \tag{C.6}$$

and define the operators that *flip* the spin:

$$\sigma_{\pm} = \frac{1}{2}(\sigma_x \pm i\sigma_y). \tag{C.7}$$

We remind that the whenever a triplet of operators satisfy the commutation relation of eq. (C.6), they have the same properties of the Pauli matrices and therefore an equivalent description may be done.

C.1.1 Collective spin states

We now proceed, following [53], in the generalization to a system composed by N particles that can be treated as a pseudo-spin. The Hilbert space $\mathscr{H}_{\mathscr{N}} \equiv \mathscr{H}_{\in}{}^{\otimes N}$ of dimension 2^N is spanned by the product states defined by:

$$\bigotimes_{i=1}^{N} |S_i\rangle,\ S_i = \uparrow, \downarrow . \tag{C.8}$$

We can define the *collective spin operators* as the sum of the individual operators:

$$J_k = \sum_{i=1}^{N} j_k^{(i)},\ k = x, y, z. \tag{C.9}$$

These collective operators satisfy the same set of commutation relations

$$[J_i, J_j] = 2i\varepsilon_{ijk}J_k,$$

and are therefore spin operators typical of $SU(2)$ and may be used to describe rotations on a Bloch sphere.

We further define the *Casimir* operator for a collective spin system:

$$\mathbf{J}^2 = J_x^2 + J_y^2 + J_z^2, \tag{C.10}$$

which commutes with all the collective spin operators J_k.

The eigenstates of the Casimir operator are called *Dicke states*[2] $|J,M\rangle$ ($0 < J < \frac{N}{2}$, $-J < M < J$) and satisfy:

$$\mathbf{J}^2|J,M\rangle = J|J,M\rangle, \tag{C.11}$$

$$J_z|J,M\rangle = M|J,M\rangle. \tag{C.12}$$

The dimension of the space $\mathscr{H}_D$ spanned by the Dicke states for N spin is:

$$dim\mathscr{H}_N = \begin{cases} \frac{1}{4}(N+1)(N+3) & N \text{ odd}, \\ \frac{1}{4}(N+2)^2 & N \text{ even}. \end{cases} \tag{C.13}$$

It is clear that for N>2 this space is smaller than $\mathscr{H}_N$, therefore the Dicke states do not form a complete base for $\mathscr{H}_N$. To complete the description we would need another quantum number related to the possible permutations of the particules. We do not discuss further this point[3] but we stress out that if the particle are indistinguishable it is sufficient, to characterize the ensemble, to know the coherence (related to $\mathbf{J}^2$) and the difference in population (related to J_z) of the collective state. Therefore the Dicke states form a basis of the Hilbert space associated with an ensemble of N indistinguishable spins. If we require that the total angular momentum is conserved and is $J = N/2$, than we can restrict the Hilbert space to the subspace $\mathscr{H}_S$ generated by the symmetrical basis $B_S = \{|J,M\rangle, -J < M < J\}$ that has dimension $N+1$.

There are some similarities of the Dicke states with the Fock states of the harmonic oscillator; the *ladder* operators $J_\pm = J_x \pm iJ_y$ allow[4] to generate all the Dicke states starting from any of them:

$$J_\pm|J,M\rangle = \sqrt{J(J+1) - M(M\pm 1)}|J,M\pm 1\rangle. \tag{C.14}$$

[2] These states are also called *angular momentum eigenstates* for obvious reasons.

[3] A detailed discussion may be found in [6] while a more linear one is in [53].

[4] In a way that reminds us the creation and annihilation operators of any armonic field.

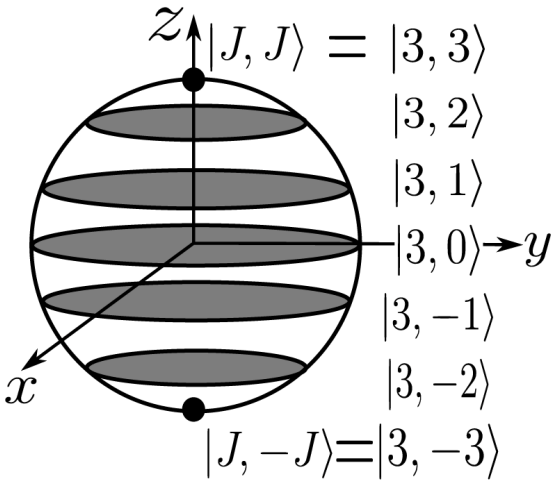

Figure C.2: Dicke states on the Bloch sphere. Image taken from [53]

The Dicke states may be represented on the Bloch sphere [6][53][5] as circles that lay parallel to the equatorial plane with latitude defined by the magnetic quantum number M. The north (south) pole here corresponds to the maximal (minimal) angular momentum eigenstate *i.e.* $|J,M = (-)J\rangle$. It is easy to see that Dicke states are invariant under rotations on the vertical axis of the Bloch sphere.

C.2 Coherent spin states

A comprehensive derivation of the *coherent spin states* (CSS) requires some attention regarding the mathematical aspects that the interested reader may find in [6][6]; nevetheless the results that are important for this work may be enounced and a representation on the Bloch sphere will be sufficient to grasp the physics.
Coherent spin states can be obtained by rotating a Dicke state through an angle

[5] And references cited therein.

[6] In this paper it may be found an interesting and detailed comparison with the states and operators of a field.

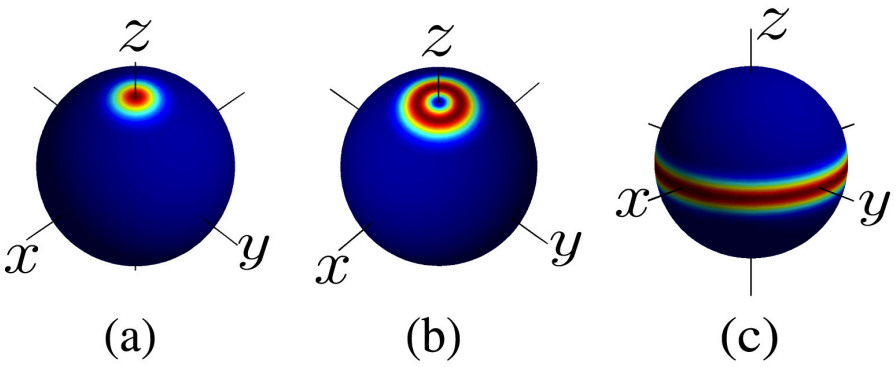

Figure C.3: Husimi representation of Dicke states on the Bloch sphere. a)$|J,-J\rangle$, b) $|J,-J+1\rangle$, c)$|J,0\rangle$. Image taken from [53]

(θ,ϕ) in angular momentum space; the decomposition of the CSS $|\theta,\phi\rangle$ on the Dicke states is then[6][53]:

$$|\theta,\phi\rangle = \sum_{M'}(-1)^{J+M'}\binom{2J}{J+M'}^{1/2} e^{-i\phi M'}\cos^{J-M'}\left(\frac{\theta}{2}\right)\sin^{J+M'}\left(\frac{\theta}{2}\right)|J,M'\rangle. \tag{C.15}$$

Two limiting cases, that are important in the study of our interest, are the $\theta=\pi/2$ and $\theta=\pi$ for $\phi=0$, that in the limit $J=N/2\gg 1$ become:

$$|\pi/2,0\rangle \approx \sum_{M'}(-1)^{J+M'}e^{-2M'^2/J}|J,M'\rangle, \tag{C.16}$$

which is a Gaussian state, and:

$$|\pi,0\rangle = |J,-J\rangle, \tag{C.17}$$

which means that the Dicke state $|J,J\rangle$ is displaced on the opposite pole.
CSS form[7] an overcomplete base that may be used to represent any collective spin state on the Bloch sphere[8]. This representation goes under the name of *Husimi Q distribution*[29]. The Husimi distribution of a Dicke state is found to be:

[7]Like the coherent field states.

[8]In an way that is similar to the representation of field states through the Wigner distribution or the Q distribution.

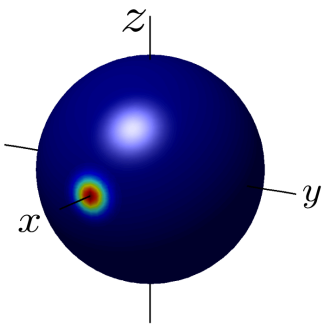

Figure C.4: Husimi representation of Coherent spin state polarized on the x axis. Image taken from [53]

$$Q_{|J,M\rangle}(\theta,\phi) = |\langle\theta,\phi|J,M\rangle|^2 = \binom{2J}{J+M}\cos^{2(J-M}\left(\frac{\theta}{2}\right)\sin^{2(J+M}\left(\frac{\theta}{2}\right), \tag{C.18}$$

which is, as one would expect, indipendent from ϕ as we have seen that Dicke states are invariant under rotations on the vertical axis (see Figure C.3).

The Husimi Q representation of a CSS, in the limit $N \gg 1$ is well approximated by a Gaussian distribution[9]:

$$Q_{|\theta'\phi'\rangle}(\theta,\phi) \approx exp\left\{-\frac{J}{2}\left[(\theta-\theta')^2+\frac{1}{2}(1-\cos 2\theta')(\phi-\phi')^2\right]\right\}. \tag{C.19}$$

The CSS for a pulse of $\pi/2$ is given by:

$$Q_{|\pi/2,0\rangle}(\theta,\phi) = \left|\left\langle\theta,\phi|\frac{\pi}{2},0\right\rangle\right|^2 = \left(\frac{+\cos\phi\sin\theta}{2}\right)^{2J}, \tag{C.20}$$

and in the limit $N \gg 1$ becomes a Gaussian symmetical on θ and ϕ (that is $\sigma_\theta = \sigma_\phi = 1/\sqrt{J}$; see Figure C.4):

$$Q_{|\pi/2,0\rangle}(\theta,\phi) \approx exp\left\{-\frac{J}{2}\left[(\theta-\pi/2)^2+\phi^2\right]\right\}. \tag{C.21}$$

[9]Exactly in the same way a coherent field state representation in the Husimi [29] and in the Wigner representation.

Appendix D

SCHEMATICS OF THE ELECTRONIC CIRCUITS

IN this appendix we report some of the schemes of the electonics boards we used and we studied in chapter 5.

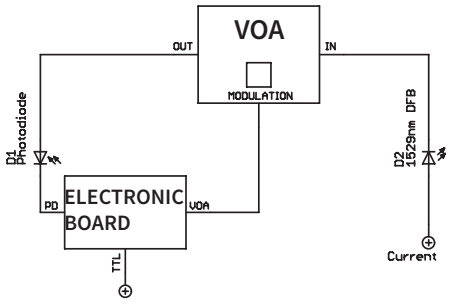

Figure D.1: Scheme of the feedback loop.

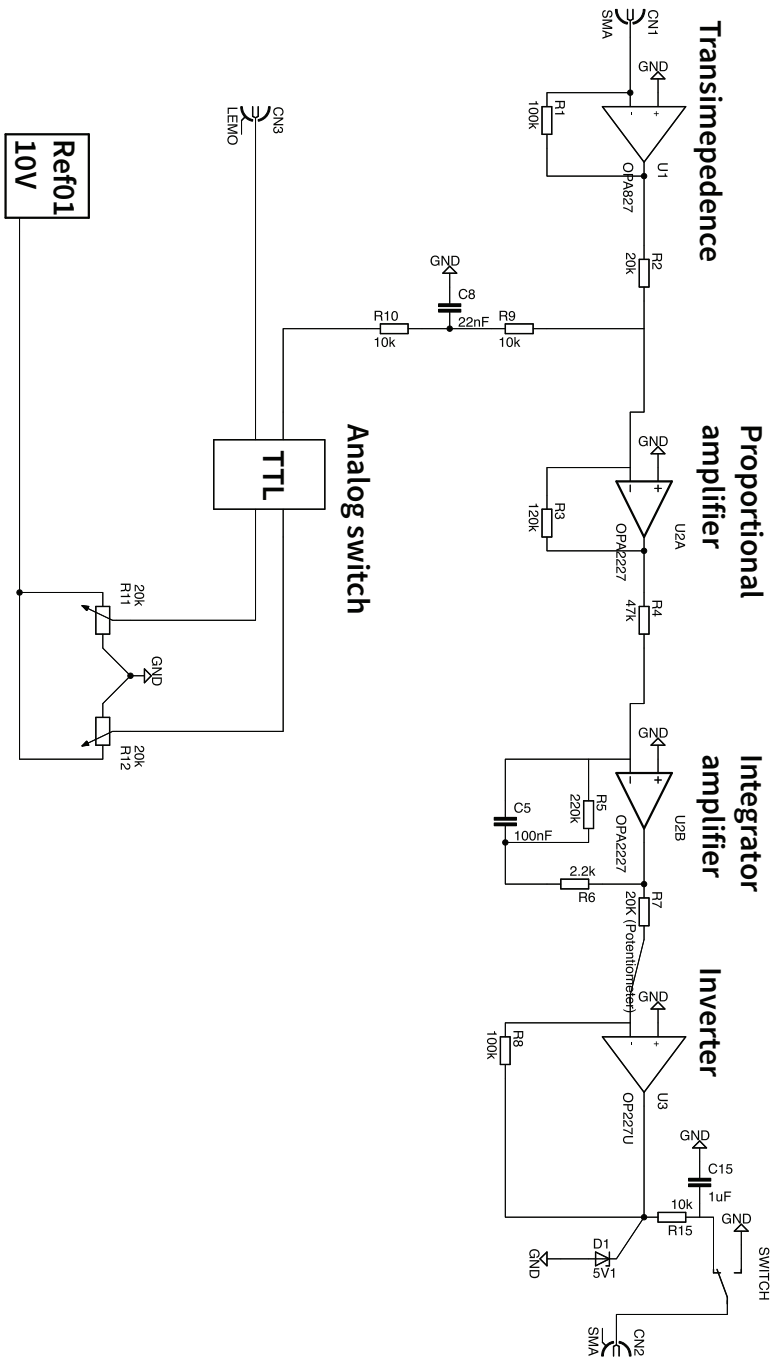

Figure D.2: Scheme of the electronic board for feedback loop.

Appendix E

LASER CHARACTERIZATION DATA

In this appendix we report the characterization of three of the lasers used in the BIARO experiment.

We characterized the RIO PLANEX 1560*nm* dfb, the Koheras AdjustiK E15 1529*nm* and the LASER 3 (1560) through the use of a optical spectrum analizer[1]. The characterization has been done of the wavelength ($\lambda peak$) as a function of the working temperature (T) and for the RIO PLANEX also of the wavelength as a function of the driving current (I_{bias}).

A characterization of this kind is required if high resolution of the wavelength is needed as in the case of BIARO experiment. The most important characterization is the one of the 1529*nm* laser since the resonance between the iperfine levels BLABLABLA.

Results of the characterization are shown in the following figures.

The laser diode has a linear response to temperature changing all along the range of temperature that can be used and also on the range we were intrested in. The linear fit[2] of the wavelength versus temperature date across all the range we

[1] inserire modello

[2] For the linear fits we used the native function in Excel for Mac 2007

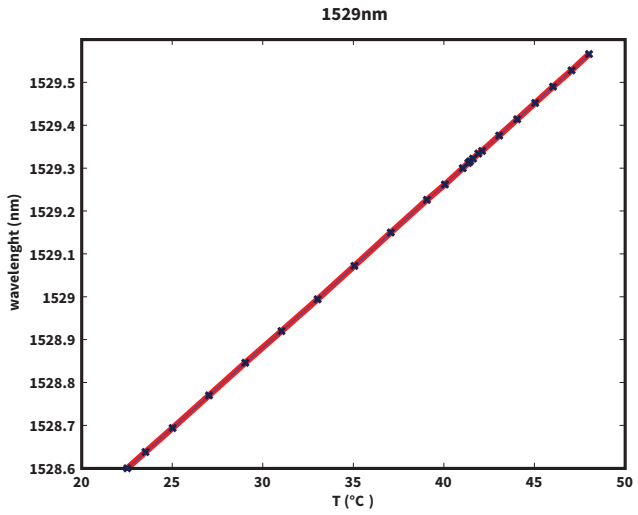

Figure E.1: Characterization of the 1529 laser. Wavelength versus temperature: full range

tested is (λ is in *nm* and T in us degrees):

$$\lambda = 0.037874T + 1527.7. \tag{E.1}$$

The resonance wavelength are 1529.24*nm* and 1529.36*nm* so it was important to know exactly how the laser diode worked in this region (see Fig:E.2). We then took more data ponits in the region of interest and did a linear fit wich gave as a result (λ is in *nm* and T in Celsius degrees)

$$\lambda = 0.038025T + 1527.7 \tag{E.2}$$

We notice that the RIO Planex diode shows an hysteresis loop (see Fig:E.3)in the wavelength VS temperature diagram wich is an interesting feature that allows to have a broader excursion in the wavelength range.
During the experiment the laser is usually used at 26.00 degrees so the wavelength VS driving current diagram is taken at that temperature (see FIG:E.4).

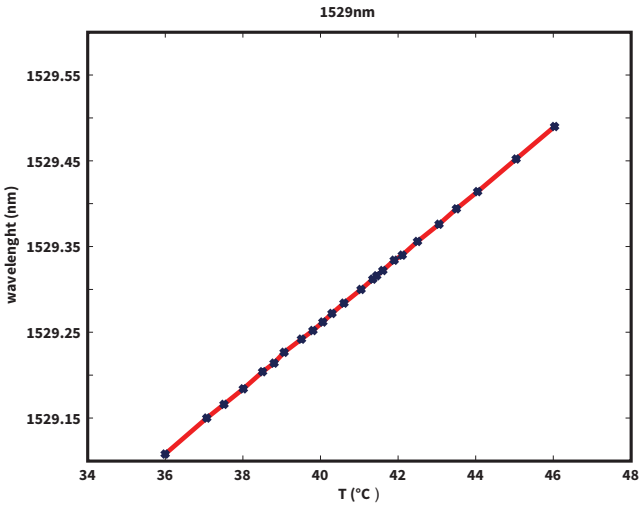

Figure E.2: Characterization of the 1529 laser. Wavelength versus temperature: resonance range

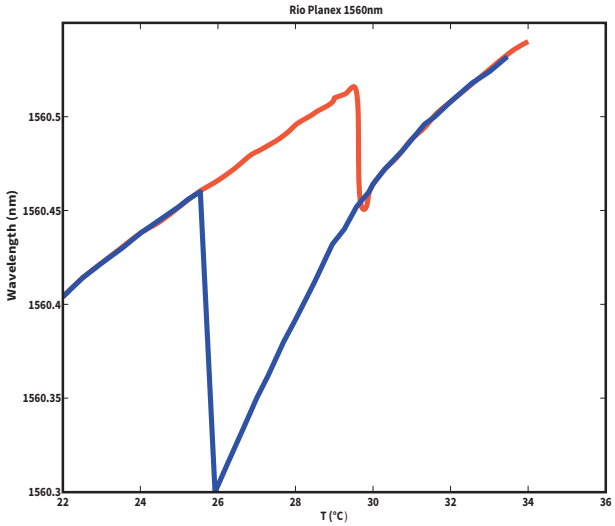

Figure E.3: Characterization of the RIO Planex 1560nm laser. Wavelength versus temperature. Measurement taken at $I_{bias} = 100mA$. In RED the ramp up; in BLUE the rap down.

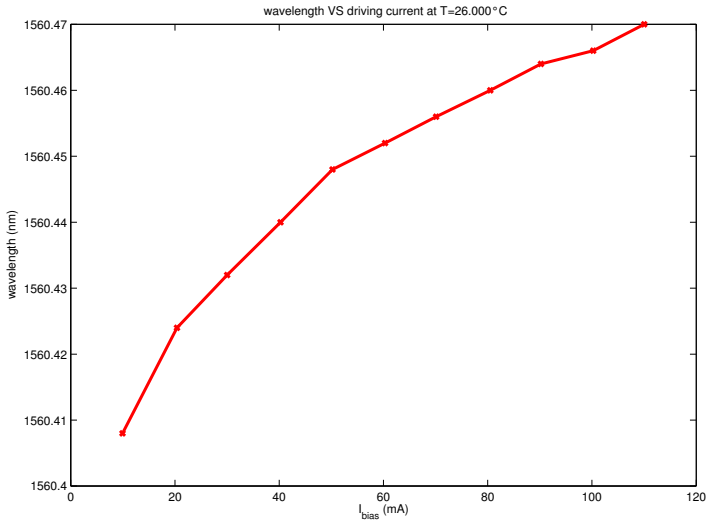

Figure E.4: Characterization of the RIO Planex 1560*nm* laser. Wavelength versus driving current. Measurement taken at $T = 26.000C$

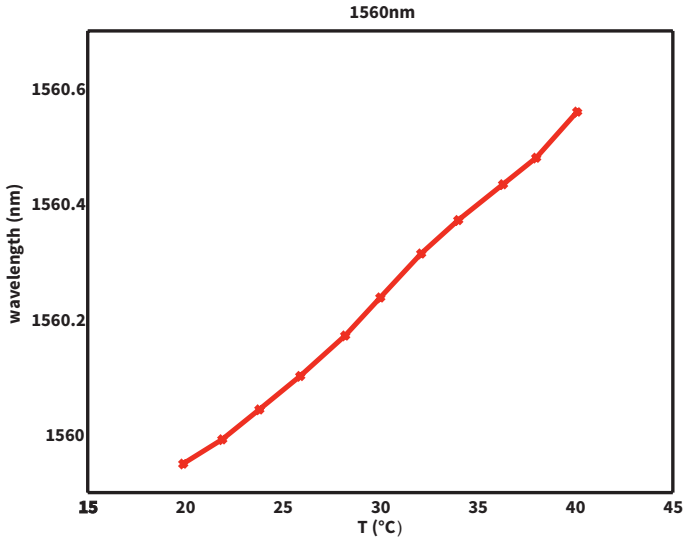

Figure E.5: Characterization of the KEOPSYS 1560*nm* laser. Wavelength versus temperature

Bibliography

[1] C. S. Adams, H. J. Lee, N. Davidson, M. Kasevich, and S. Chu. Evaporative cooling in a crossed dipole trap. *Phys. Rev. Lett.*, 74:3577–3580, 1995.

[2] Y. Aharonov, D. Albert, and L. Vaidman. How the result of a measurement of a component of the spin of a spin-1/2 particle can turn out to be 100. *Physical Review Letters*, 60(14):1351–1354, 1988.

[3] Y. Aharonov and L. Vaidman. Properties of a quantum system during the time interval between two measurements. *Physical Review A*, 41(1):11–20, 1990.

[4] M.H. Anderson, J.R. Ensher, W.R. Matthews, C. E. Wieman, and E. A. Cornell. Observation of Bose-Einsten Condensation in a DIlute Atomic Vapor. *Science1995*, 269:51–54, 1955.

[5] J.F. Annett. *Superconductivity, Superfluids and Condensates*. Oxford University Press, 2004.

[6] F.T. Arecchi, R. Gilmore, E. Courtens, and H. Thomas. Atomic Coherent States in Quantum Optics. *Physical Review A*, 6(6), 1972.

[7] A. Ashkin. *Optical Trapping and Manipulation of Neutral Particles Using Lasers*. World Scientific Publishing, 2006.

[8] S. Bernon. *Trapping and nondemolition measurement of cold atoms in a high-finesse ring cavity*. PhD thesis, Ecole Polytechnique, 2011.

[9] S. Bernon, T. Vanderbruggen, R. Kohlhaas, A. Bertoldi, A. Landragin, and P. Bouyer. Heterodyne non-demolition measurements on cold atomic samples: towards the preparation of non-classical states for atom interferometry. *New Journal of Physics*, 13(6), 2011.

[10] A. Bertoldi, S. Bernon, T. Vanderbruggen, A. Landragin, and P. Bouyer. In situ characterization of an optical cavity using atomic light shift. *Optics letters*, 35(22):3769–71, 2010.

[11] D. Bhattacharyya, B. K. Dutta, B. Ray, and P. N. Ghosh. Line shape simulation and saturated absorption spectroscopic measurement of Rb-D2 transition. *Chemical Physics Letters*, 389(1-3):113–118, May 2004.

[12] T. Boaz and C. Eliahu. Introduction to Weak Measurements and Weak Values. *Quanta*, 2:7–17, 2013.

[13] V. Braginsky and F. Khalili. Quantum nondemolition measurements: the route from toys to tools. *Reviews of Modern Physics*, 68(1):1–11, 1996.

[14] V. Braginsky, Y.I Vorontsov, and K. S. Thorne. Quantum Nondemolition Measurements. *Science*, 209(4456):547–557, 1980.

[15] J. Brantut, J. Clement, M. de Saint Vincent, G. Varoquaux, R. Nyman, Alain Aspect, T. Bourdel, and P. Bouyer. Light-shift tomography in an optical-dipole trap for neutral atoms. *Physical Review A*, 78(3):78–81, 2008.

[16] A. Cho. Physics. Furtive approach rolls back the limits of quantum uncertainty. *Science (New York, N.Y.)*, 333(6043):690–3, 2011.

[17] A. A. Clerk, S. M. Girvin, Florian Marquardt, and R. J. Schoelkopf. Introduction to quantum noise, measurement, and amplification. *Reviews of Modern Physics*, 82(2):1155–1208, 2010.

[18] C Cohen-Tannoudji and S Reynaud. Dressed-atom description of resonance fluorescence and absorption spectra of a multi-level atom in an intense laser

beam. *Journal of Physics B: Atomic and Molecular Physics*, 10(3):345–363, 1977.

[19] C. N. Cohen-tannoudji. Manipulating atoms with photons . *Reviews of Modern Physics*, 70(3):707–719, 1998.

[20] C. N. Cohen-tannoudji and B. Laloe. *Quantum Mechanics*. Wiley, 1992.

[21] A. D. Cronin, D. E. Pritchard, and J. Schmiedmayer. Optics and interferometry with atoms and molecules. *Reviews of Modern Physics*, 81(3):1051–1129, 2009.

[22] F. Dalfovo, S. Giorgini, L. P. Pitaevskii, and S. Stringari. Theory of bose-einstein condensation in trapped gases. *Rev. Mod. Phys.*, 71:463–512, Apr 1999.

[23] J. Dalibard and C. N. Cohen-Tannoudji. Dressed-atom approach to atomic motion in laser light: the dipole force revisited. *Journal of the Optical Society of America B*, 2(11):1707, 1985.

[24] K.B. Davis, M.-O Mewes, M.R. Andrews, N.J. van Druten, D.S. Durfee, D.M. Kurn, and W. Ketterle. Bose-Einstein Condensation in a Gas of Sodium Atoms. *Physical Review Letters*, 75(November), 1995.

[25] R.W.P. Drever, J.L. Hall, F.V. Kowalski, J. Hough, G.M. Ford, A.J. Munley, and H. Ward. Laser Phase and Frequency Stabilization Using an Optical Resonator. *Applied Physics B*, 31:97–105, 1983.

[26] S. Echaniz, M. W. Mitchell, M. Kubasik, M. Koschorreck, H. Crepaz, J. Eschner, and E. S. Polzik. Conditions for spin squeezing in a cold 87 Rb ensemble. *Journal of Optics B: Quantum and Semiclassical Optics*, 7(12):S548–S552, 2005.

[27] R. Grimm, M. Weidemuller, and Y. B. Ovchinnikov. Optical dipole traps for neutral atoms. *Arxiv*, pages 1–39, 1999.

[28] L. Hardy. Quantum mechanics, local realistic theories, and lorentz-invariant realistic theories. *Phys. Rev. Lett.*, 68:2981–2984, May 1992.

[29] S. Haroche and J.M. Raimond. *Exploring the Quantum: Atoms, Cavities, and Photons*. Oxford University Press, 2006.

[30] P.C.D. Hobbs. Photodiode Front Ends: The REAL Story. *Optics and Photonics News*, pages 42–45, 2001.

[31] M. Hofheinz, E. M. Weig, M. Ansmann, R. C. Bialczak, E. Lucero, M. Neeley, A. D. O'Connell, H. Wang, J. M Martinis, and A. N. Cleland. Generation of Fock states in a superconducting quantum circuit. *Nature*, 454(7202):310–4, 2008.

[32] K. Huang. *Statistical Mechanics*. John Wiley & Sons, 2 edition, 1987.

[33] M. Kasevich and S. Chu. Laser Cooling below a Photon Recoil with Three-Level Atoms. *Physical Review Letters*, 69(12):1741–1745, 1992.

[34] A. J. Kerman, V. Vuletić, C. Chin, and S. Chu. Beyond optical molasses: 3d raman sideband cooling of atomic cesium to high phase-space density. *Phys. Rev. Lett.*, 84:439–442, 2000.

[35] S. Kocsis, B. Braverman, S. Ravets, M. J. Stevens, R. P. Mirin, L. K. Shalm, and A. M Steinberg. Observing the average trajectories of single photons in a two-slit interferometer. *Science (New York, N.Y.)*, 332(6034):1170–3, 2011.

[36] H. Kogelnik and T Li. Laser beams and resonators. *Applied Optics*, 5(10):1550–1567, 1966.

[37] R. Kohlhaas, T. Vanderbruggen, S. Bernon, A. Bertoldi, A. Landragin, and P. Bouyer. Robust laser frequency stabilization by serrodyne modulation. *Optics letters*, 37(6):1005–7, 2012.

[38] A. Kuzmich, N. P. Bigelow, and L. Mandel. Atomic quantum non-demolition measurements and squeezing. *Europhysics Letters*, 42(5):481–486, 1998.

[39] Seth Lloyd and Jean-Jacques E. Slotine. Quantum feedback with weak measurements. *Physical Review A*, 62(1), 2000.

[40] J. S. Lundeen, B. Sutherland, A. Patel, C. Stewart, and C. Bamber. Direct measurement of the quantum wavefunction. *Nature*, 474(7350):188–91, June 2011.

[41] A. Lupascu, S. Saito, T. Picot, P. C. de Groot, C. J. P. M. Harmans, and J. E. Mooij. Quantum non-demolition measurement of a superconducting two-level system. *Nature Physics*, 3(2):119–125, 2007.

[42] A. Messiah. *Quantum Mechanics (2 Volumes in 1)*. Dover Publications, 1999.

[43] J.H. Metcalf and P van der Straten. *Laser Cooling and Trapping*. Springer, 1999.

[44] G. Nogues, A. Rauschenbeutel, S. Osnaghi, and M. Brune. Seeing a single photon without destroying it. *Nature*, 400:239–242, 1999.

[45] W. D. Phillips. Laser cooling and trapping of neutral atoms. *Reviews of Modern Physics*, 70(3):721–741, 1998.

[46] Proceedings of Xth International Conference on Thermoelectrics. *Reliability of thermoelectric cooling systems*, Cardiff, 1991.

[47] Isidor Isaac Rabi. Space Quantization in a Gyrating Magnetic Field. *Physical Review*, 51:652–654, 1937.

[48] D. E. Rivera, M. Morari, and S. Skogestad. Internal model control: PID controller design. *Industrial & Engineering Chemistry Process Design and Development*, 25(1):252–265, January 1986.

[49] K.C. Robinson. VARIABLE OPTICAL ATTENUATOR, 2000.

[50] T. A. Savard and J. E. Thomas. Laser-noise-induced heating in far-off resonance optical traps. *Physical Review A*, 56(2), 1997.

[51] C. Sayrin, I. Dotsenko, X. Zhou, B. Peaudecerf, T. Rybarczyk, S. Gleyzes, P. Rouchon, M. Mirrahimi, H. Amini, M. Brune, J. M. Raimond, and S. Haroche. Real-time quantum feedback prepares and stabilizes photon number states. *Nature*, 477(7362):73–7, 2011.

[52] T. Vanderbruggen. Vers la condensation de Bose-Einstein dans un résonateur optique de haute finesse. Technical report, Universite de Paris-Sud, 2008.

[53] T. Vanderbruggen. *Detection non-destructive pour l'interferometrie atomique et Condensation de Bose-Einstein dans une cavite optique de haute finesse*. PhD thesis, Universite de Paris-Sud, 2012.

[54] T. Vanderbruggen, S. Bernon, A. Bertoldi, A. Landragin, and P. Bouyer. Spin-squeezing and Dicke-state preparation by heterodyne measurement. *Physical Review A*, 83(1), 2011.

[55] T. Vanderbruggen, R. Kohlhaas, A. Bertoldi, S. Bernon, A. Aspect, A. Landragin, and P. Bouyer. Feedback control of trapped coherent atomic ensemble. *Physical Review Letters*, 110(21), 2013.

[56] J. Von Neumann. *Mathematical foundations of quantum mechanics*. Princeton University Press, 1996.

[57] V. Vuletić, C. Chin, A. Kerman, and S. Chu. Degenerate Raman Sideband Cooling of Trapped Cesium Atoms at Very High Atomic Densities. *Physical Review Letters*, 81(26):5768–5771, December 1998.

[58] K. Yokota, T. Yamamoto, M. Koashi, and N. Imoto. Direct observation of Hardy's paradox by joint weak measurement with an entangled photon pair. *New Journal of Physics*, 11(3):1–10, March 2009.

Acknowledgements

Desidero ringraziare prima di tutto Andrea Bertoldi che ha supervisionato il mio lavoro di tesi e mi ha insegnato tutto quello che ho imparato sulla materia con tanta pazienza. Andrea mi ha fornito consigli scientifici e di vita che, sono sicuro, mi saranno sempre preziosi. Un grazie anche ai membri del gruppo con cui ho condiviso i mesi parigini e che mi sono stati di supporto costante: Ralf Kohlhaas, Etienne Cantin e Thomas Vanderbruggen. Per gli insegnamenti pratici nel campo dell'elettronica un grazie a Frédéric Moron. Infine un ringraziamento immenso a Elisa Ercolessi, paziente e scupolosa relatrice, ma soprattutto la migliore insegnante che io abbia avuto la fortuna di incontrare nei miei (troppi) anni universitari.

In questi tre anni di laurea tante persone mi sono state vicino, alcune di passaggio, alcune presenze costanti. So che dimenticherò qualcuno, forse molti, ma desidero esprimere i miei ringraziamenti a: il Barbe per la sua presenza costante nei mesi di scrittura. Senza di lui non sarebbe stato così piacevole concludere questo lavoro. Bobo per il suo supporto perenne, gratuito e sempre affidabile. Edo che con il suo viso scuro mi ricorda sempre che la vita non dovrebbe essere fatta di chiacchiere da bar, ma in fondo lo è. Tix, che ha reso i pomeriggi di studio (mai le mattine) un momento da passare in compagnia, sempre piacevole, sempre stimolante. Tutti i fisici, che nel loro andare e venire da Bologna, hanno più spesso offerto un pretesto per non studiare piuttosto che una compagnia di studio. Piero, che vorrei sapesse che lo stimo molto per le sue scelte. I colleghi di Ducati, in particolare Chiara, Alessandro e David, per avermi fatto vivere un periodo bellissimo

in un contesto veramente affascinante. Gli amici del bar Belmeloro, luogo di fine e inizio giornata per diversi mesi. I compagni dei mille calcetti e del fantacalcio, spesso più di uno svago della domenica. Un grazie agli amici storici: Pilu, Robby, Morga, Tabe, Claudia, Jessica, Eleonora, Bucci, Mitch, Emi, Eugenio, Annalisa, Dimitri, Peppo, Rudi, Sara, Arianna, Marco, Barto, Fabio, Andrea, Lucia, Zulia e tutti quelli che dimentico.

L'ultimo ringraziamento va alle tre persone che più di tutte mi hanno fatto amare questa materia: Carlo Bertoni, per avermi dato il primo esempio di come avrei voluto essere "da grande". Carlo Rovelli, per avermi mostrato quanto la passione possa portare lontano ed Ettore Remiddi per avermi insegnato a ragionare in maniera critica.